ALZHEIMER'S DISEASE

Tau reduction prevents neuronal loss and reverses pathological tau deposition and seeding in mice with tauopathy

Sarah L. DeVos,[1] Rebecca L. Miller,[1]* Kathleen M. Schoch,[1]* Brandon B. Holmes,[1] Carey S. Kebodeaux,[1] Amy J. Wegener,[1] Guo Chen,[1] Tao Shen,[1] Hien Tran,[2] Brandon Nichols,[2] Tom A. Zanardi,[2] Holly B. Kordasiewicz,[2] Eric E. Swayze,[2] C. Frank Bennett,[2] Marc I. Diamond,[3] Timothy M. Miller[1†]

Accumulation of hyperphosphorylated tau directly correlates with cognitive decline in Alzheimer's disease and other primary tauopathies. One therapeutic strategy may be to reduce total tau expression. We identified antisense oligonucleotides (ASOs) that selectively decreased human tau mRNA and protein in mice expressing mutant P301S human tau. After reduction of human tau in this mouse model of tauopathy, fewer tau inclusions developed, and preexisting phosphorylated tau and Thioflavin S pathology were reversed. The resolution of tau pathology was accompanied by the prevention of hippocampal volume loss, neuronal death, and nesting deficits. In addition, mouse survival was extended, and pathological tau seeding was reversed. In nonhuman primates, tau ASOs distributed throughout the brain and spinal cord and reduced tau mRNA and protein in the brain, spinal cord, and cerebrospinal fluid. These data support investigation of a tau-lowering therapy in human patients who have tau-positive inclusions even after pathological tau deposition has begun.

INTRODUCTION

Tau is a microtubule-associated protein capable of binding to microtubules in the neuron, but when subjected to pathogenic conditions, aggregates and toxic oligomers form, resulting in intraneuronal neurofibrillary tangles (NFTs). An early histopathologic marker of Alzheimer's disease (AD) is the presence of NFTs in the entorhinal cortex that appear to traverse through the brain along neural networks to the hippocampus, neocortex, and, ultimately, the rest of the brain (*1*). Damage to these neuronal connections is hypothesized to underlie memory loss in AD patients and may be one of the first steps toward widespread neuronal loss and dementia (*2*).

The close correlation between tau deposition and cognitive decline (*3*) along with genetic evidence that tau mutations cause widespread neurodegeneration in patients with frontotemporal dementia (FTD) with parkinsonism linked to chromosome 17 (FTDP-17) strongly supports the development of therapies targeting tau. Although several therapies that target the tau disease pathway have been tested—such as disrupting tau misfolding (*4*), targeting tau acetylation (*5*), inhibiting tau-induced proteasome impairment (*6*), and tau immunotherapy (*7*–*11*)—none of these target tau mRNA with the goal of reducing total human tau expression. In mice, genetic ablation of endogenous tau is well tolerated with a minor motor phenotype developing only after 12 to 16 months (*12*–*14*). Our group has previously shown that endogenous murine tau reduction in adult mice results in no behavioral or neuroanatomical abnormalities, supporting the viability of a tau-lowering therapy (*15*).

To study the therapeutic effects of a human tau reduction strategy in a mouse model of human tauopathy, we developed antisense oligonucleotides (ASOs) that selectively reduced human tau expression throughout the adult mouse brain. Similar ASO mRNA-targeted approaches have improved disease phenotypes in rat models of superoxide dismutase 1 (SOD1)–related amyotrophic lateral sclerosis (ALS) (*16*), mouse models of Huntington's disease (*17*) and FTDP-17 (*18*), and C9ORF72 patient-derived cell lines (*19*, *20*). Administering SOD1 ASOs into the central nervous system (CNS) of human ALS patients via the cerebrospinal fluid (CSF) has been well tolerated (*21*). We tested these tau-reducing ASOs in PS19 mice carrying human tau with the P301S mutation (*22*) and found beneficial effects on tau deposition, neuronal survival, tau seeding, and mouse survival.

RESULTS

Human tau ASOs reduce human tau mRNA in mice

Human tau ASOs were designed to be specific for human tau and targeted the coding 1N4R transgene of human tau expressed in the PS19 mouse model, which expresses human tau carrying the P301S mutation (*22*). Before testing human tau ASOs, we tested whether a scrambled ASO with the same chemistry would alter human tau or murine tau mRNA expression at several time points after ASO administration. PS19 mice treated with saline vehicle or scrambled ASO (30 μg/day for 28 days; total, 840 μg) were tested at 4, 8, and 12 weeks after implantation of a pump for ASO delivery, and both human tau and murine tau mRNA were measured. No significant differences were seen at any of the time points for either human tau [one-way analysis of variance (ANOVA), Sidak post hoc analysis: 4 weeks, $P = 0.968$; 8 weeks, $P = 0.926$; 12 weeks, $P = 0.331$)] or murine tau (one-way ANOVA, Sidak post hoc analysis: 4 weeks, $P = 0.948$; 8 weeks, $P = 0.824$; 12 weeks, $P = 0.501$) mRNA (fig. S1).

We next tested the duration of action of the human tau–specific ASO ($Tau^{ASO\text{-}12}$) in preparation for a 3-month treatment to reduce human tau. Alzet osmotic pumps were implanted in PS19 mice, allowing for slow infusion over 28 days of a control [saline vehicle or scrambled ASO (30 μg/day), total, 840 μg] treatment (4 weeks, $n = 10$; 8 weeks, $n = 5$; 12 weeks $n = 8$) or $Tau^{ASO\text{-}12}$ human tau reduction treatment (30 μg/day;

[1]Department of Neurology, Hope Center for Neurological Disorders, Washington University in St. Louis, St. Louis, MO 63110, USA. [2]Ionis Pharmaceuticals, Carlsbad, CA 90201, USA. [3]Center for Alzheimer's and Neurodegenerative Diseases, University of Texas Southwestern Medical Center, Dallas, TX 75390, USA.
*These authors contributed equally to this work.
†Corresponding author. Email: miller.t@wustl.edu

total, 840 μg; 4 weeks, $n = 3$; 8 weeks, $n = 5$; 12 weeks, $n = 11$). Total human tau mRNA was significantly reduced at 4, 8, and 12 weeks after pump implantation in Tau^{ASO-12}–treated mice (Fig. 1A) (two-way ANOVA, $F_{1,43} = 22.96$, $P < 0.0001$; Bonferroni post hoc analysis: 4 weeks, $P = 0.0250$; 8 weeks, $P = 0.0448$; 12 weeks, $P < 0.0001$). Murine tau mRNA was not significantly altered (Fig. 1B) (two-way ANOVA, $F_{1,43} = 1.27$, $P = 0.267$; Bonferroni post hoc analysis: 4 weeks, $P = 0.265$; 8 weeks, $P > 0.999$; 12 weeks, $P > 0.999$). There was no difference in either human tau (two-tailed Student's t test, $P = 0.703$) or murine tau (two-tailed Student's t test, $P = 0.496$) mRNA between saline and scrambled ASO control treatments, and thus, these values were combined as single control values. The long duration of target mRNA reduction seen here corresponds with studies using similar ribonuclease H (RNase H) ASOs (*15*, *17*). Thus, a 1-month infusion of scrambled ASO or Tau^{ASO-12} at 30 μg/day was selected in all subsequent studies to ensure 12 weeks of human tau mRNA reduction.

ASOs are distributed throughout the adult murine brain

After 1 month of saline or ASO infusion at 30 μg/day followed by an 8-week washout period, mouse brains were stained for the ASO itself using an antibody that recognized the backbone chemistry of ASOs, regardless of sequence (*15*, *17*). Tau^{ASO-12} diffused throughout the mouse brain and visibly persisted to the end of the 12-week treatment period (Fig. 1C and fig. S2) (*15*, *17*).

Tau ASO treatment prevents AT8-positive tau deposition

Tau pathology first deposits at 5 to 6 months of age in PS19 mice. To assess whether Tau^{ASO-12} can prevent pathology from developing, we administered scrambled ASO ($n = 5$) or Tau^{ASO-12} ($n = 10$) at 6 months of age. Pumps were removed 1 month after implantation, and mouse brain tissue was collected 2 months later. Age-matched nontransgenic littermate controls were treated with scrambled ASO ($n = 7$). Human tau mRNA (one-way ANOVA, Sidak post hoc analysis, $P = 0.004$; fig. S3A) and human tau protein (one-way ANOVA, Sidak post hoc analysis, $P = 0.011$; Fig. 1D) were significantly reduced in the Tau^{ASO-12} group compared to the

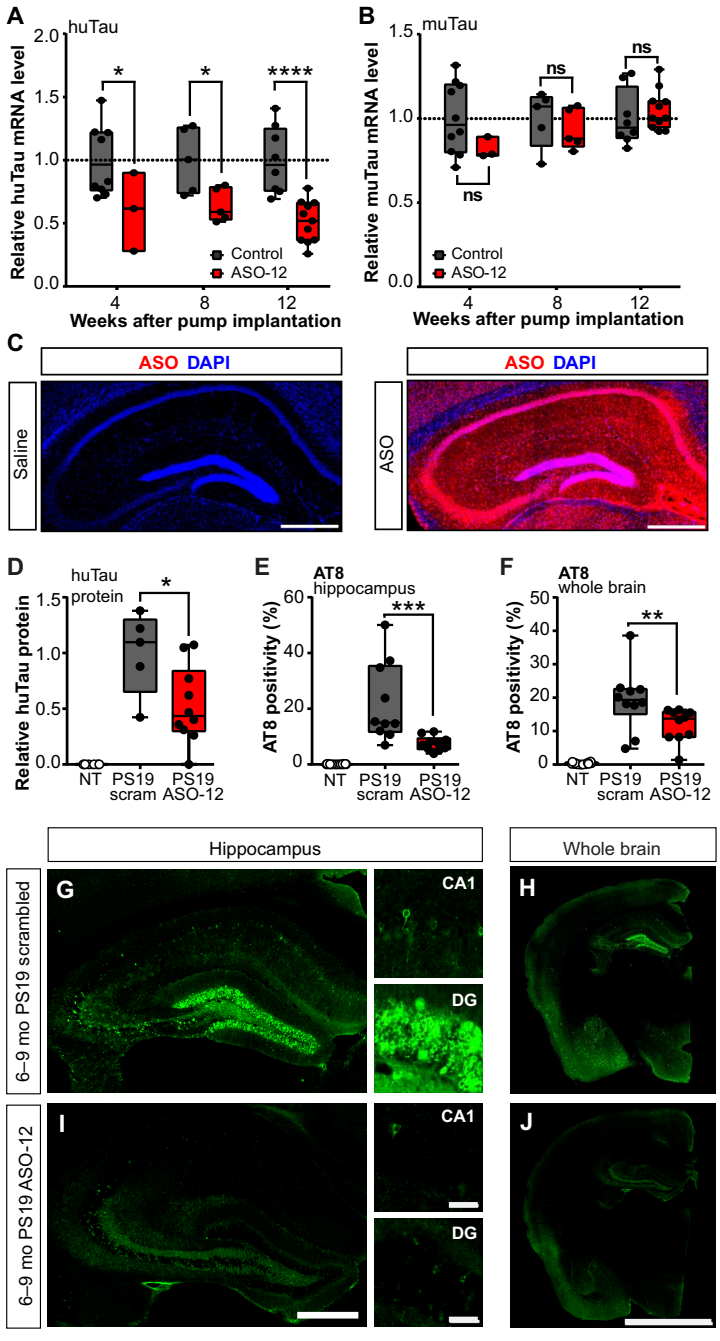

Fig. 1. ASOs reduce human tau and prevent tau pathology in vivo. (**A** and **B**) Saline, scrambled ASO, or Tau^{ASO-12} was delivered via intracerebroventricular (ICV) infusion at 30 μg/day for 1 month into 3- to 6-month-old adult PS19 mice. Human tau (huTau) (A) and mouse tau (muTau) (B) mRNA were analyzed at 4 (control, $n = 10$; Tau^{ASO-12}, $n = 3$), 8 (control, $n = 5$; Tau^{ASO-12}, $n = 5$), and 12 (control, $n = 8$; Tau^{ASO-12}, $n = 11$) weeks after pump implantation and ASO delivery (two-way ANOVA, Bonferroni post hoc analysis). n.s., not significant. (**C**) Mouse brains collected 12 weeks after pump implantation were stained with an ASO antibody (red) and counterstained with nuclear stain DAPI (blue) on the contralateral hemisphere of the catheter. ASO was found throughout the entire hippocampus and brain (see also fig. S2). Scale bars, 500 μm. (**D**) PS19 mice at 6 months of age were treated with scrambled (scram) ASO (30 μg/day; $n = 5$) or Tau^{ASO-12} ($n = 10$) for 1 month [scrambled-treated nontransgenic (NT) was the control, $n = 7$]. Pumps were removed after 1 month, and mouse brain tissue was collected 2 months later. Total human tau protein was reduced in the Tau^{ASO-12} group. (**E** and **F**) ImageJ threshold quantification of AT8 positivity in the mouse hippocampus (E) and whole brain (F) showed a reduction in AT8 in the Tau^{ASO-12}–treated mice. (**G** to **J**) Representative images of AT8 tau pathology from 6- to 9-month-old treated PS19 mice. Scale bars, 500 μm (hippocampal panel), 50 μm [CA1, dentate gyrus (DG) panels], and 2.5 mm (whole brain) (one-way ANOVA, Sidak post hoc analysis). *$P < 0.05$, **$P < 0.01$, ***$P < 0.001$, ****$P < 0.0001$. Graphical data are represented as box and whisker plots with individual points overlaid, where error bars represent maximum and minimum values and the boxed line represents the median.

scrambled control group. Brains were then stained with the phospho-tau antibody AT8. PS19 mice treated with scrambled ASO showed extensive AT8-positive tau deposition by 9 months of age, particularly in the hippocampus and entorhinal/piriform cortex (Fig. 1, G and H). Tau^{ASO-12} treatment greatly reduced the amount of AT8 tau pathology deposition in the hippocampus (one-way ANOVA, Sidak post hoc analysis, $P = 0.0003$; Fig. 1, E and I) and whole-brain sections (one-way ANOVA, Sidak post hoc analysis, $P = 0.008$; Fig. 1, F and J).

Tau ASO treatment reverses tau inclusions in aged PS19 mice

To test whether reducing total human tau could reverse preexisting tau aggregates, we treated 9-month-old PS19 mice with scrambled (30 μg/day; $n = 6$) or Tau^{ASO-12} ($n = 6$) ASO for 1 month, followed by a 2-month washout period (nontransgenic control group, $n = 5$). In this older cohort, human tau mRNA ($P = 0.0003$, one-way ANOVA, Sidak post hoc analysis; fig. S3B) as well as total human tau protein were significantly reduced after Tau^{ASO-12} treatment ($P = 0.024$, one-way ANOVA, Sidak post hoc analysis; Fig. 2A). Further, we examined sarkosyl insoluble tau and found a significant decrease in total insoluble tau in Tau^{ASO-12}–treated aged PS19 mice ($P = 0.006$, two-tailed t test; Fig. 2, B and C). The lysate was further analyzed using semi-denaturing detergent agarose gel electrophoresis (SDD-AGE) to determine whether high–molecular weight (HMW) tau oligomers were also reduced. Lysate from 9- to 12-month-old treated PS19 mice was run on SDD-AGE and probed for total tau and PHF-1–positive phospho-tau (recognizing pS396/pS404) (Fig. 2, D to H). There was a reduction in total HMW total tau ($P = 0.004$, two-tailed t test) and phospho-tau ($P = 0.0104$, two-tailed t test) oligomers in the Tau^{ASO-12}–treated mice.

PS19 mice at 9 months of age also showed extensive AT8 tau pathology throughout the hippocampus and cortex. This baseline pathology enabled a direct comparison of 9- to 12-month-old treated mice with the 9-month starting point to determine whether tau pathology could be reversed. Nine- to 12-month-old PS19 mice treated with Tau^{ASO-12} showed substantially less AT8 staining in the hippocampus and the whole brain compared to both age-matched 12-month-old PS19 mice treated with scrambled ASO and untreated mice (one-way ANOVA, Sidak post hoc analysis: hippocampus, $P < 0.0001$; whole brain, $P < 0.0001$), as well as the 9-month-old PS19 mice starting group (one-way ANOVA, Sidak post hoc analysis: hippocampus, $P = 0.028$; whole brain, $P = 0.011$) (Fig. 2, I to P, and fig. S4). These data suggested that, when total human tau was reduced, preexisting neuronal aggregates of tau could be cleared from neurons in vivo. When stained for NFTs using Thioflavin S, a similar pattern emerged with Tau^{ASO-12}–treated PS19 mice showing a reversal of NFT pathology (one-way ANOVA, Sidak post hoc analysis: 9- to 12-month-old PS19 ASO-12 versus 6- to 9-month-old PS19 scrambled ASO, $P = 0.0486$; 9- to 12-month-old PS19 ASO-12 versus 9- to 12-month-old PS19 scrambled ASO, $P = 0.0078$) (Fig. 2Q and fig. S5, quantification).

In addition to measuring tau pathology burden, we stained for glial fibrillary acidic protein (GFAP) as a means to assess inflammation. Inflammation has been implicated in the pathogenesis of AD (*23*, *24*), and the PS19 mouse model has been shown to develop an age-dependent increase in the activation of astrocytes and GFAP expression (*22*, *25*). In PS19 mice treated with Tau^{ASO-12}, GFAP staining was substantially reduced as compared to 12-month-old untreated PS19 mice (fig. S6, A to C).

Hippocampal volume and neuronal loss are prevented after human tau reduction

PS19 mice show an age-dependent decrease in total hippocampal volume and increase in hippocampal neuron loss (*7*, *22*), first evident at 9 months of age. In 9- to 12-month-old Tau^{ASO-12}–treated PS19 mice, further hippocampal volume and entorhinal cortex area loss were prevented when compared to 9- to 12-month-old PS19 mice treated with scrambled ASO (hippocampus, $P = 0.009$, one-way ANOVA, Sidak post hoc analysis; entorhinal cortex, $P < 0.0001$, one-way ANOVA, Sidak post hoc analysis) (Fig. 3, A and C, and fig. S7). To determine whether prevention of hippocampal volume loss was secondary to prevention of neuronal loss, we counted 4′,6-diamidino-2-phenylindole (DAPI) (blue) and NeuN (red; a marker for neurons) dual-positive cells in the CA1 region of the hippocampus (Fig. 3, B and D) and cell size area in CA1 (fig. S8). We confirmed prevention of further neuronal loss as measured by NeuN-positive cell counts in the hippocampus after treatment with Tau^{ASO-12} in aged PS19 mice (DAPI and NeuN dual-positive cells: $P = 0.005$, one-way ANOVA, Sidak post hoc analysis; cell size: $P < 0.0001$, one-way ANOVA, Sidak post hoc analysis).

Reducing human tau prevents and reverses tau seeding capability

Recent studies have demonstrated the ability of tau to propagate from one cell to another in vitro (*26*) and from one brain region to another along synaptically connected networks in vivo (*27*, *28*). This tau "spreading" may be a mechanism for disease progression in AD and other tauopathies (*29*). One in vitro measure of the ability of pathological tau aggregates to induce misfolding of naïve monomeric tau, that is, tau "seeding" activity, is a cell-based assay that relies on flow cytometry detection of Förster resonance energy transfer (FRET). FRET can be created by intracellular aggregation of endogenously expressed repeat domain of tau (TauRD) fused with cyan fluorescent protein (TauRD-CFP) and yellow fluorescent protein (TauRD-YFP) in stably expressing human embryonic kidney (HEK) 293 cells (Fig. 4A) (*30*, *31*). Using TauRD-CFP/TauRD-YFP expressing HEK-293 cells, when cells were nontransfected or treated with nontransgenic brain homogenate lysate, only diffuse homogeneous background fluorescence and no FRET-positive inclusions were seen (Fig. 4, B and C). Upon addition of brain lysate from the 6- to 9-month-old and 9- to 12-month-old PS19 treatment cohorts, intracellular TauRD-CFP/TauRD-YFP aggregates were seen at 24 hours after lysate was applied. Tau^{ASO-12} treatment prevented tau aggregate formation in both 6- to 9-month-old and 9- to-12-month-old age groups (Fig. 4, D to G) (one-way ANOVA, Sidak post hoc analysis: 6- to 9-month-old mice, $P < 0.0001$; 9- to 12-month-old mice, $P = 0.0061$). In addition, when compared to the starting age of 9 months, tau seeding activity was reversed in the 9- to 12-month-old PS19 cohort treated with Tau^{ASO-12} ($P = 0.044$, one-way ANOVA, Sidak post hoc analysis) (Fig. 4H). These data demonstrate that tau seeding activity is substantially reduced and partially reversed by treatment with tau ASO.

Lowering human tau prolongs mouse survival and rescues nesting deficits

Hindlimb paralysis in PS19 mice begins at about 9 to 10 months of age, leading to shortened survival time (*22*). We treated 9-month-old PS19 mice with either scrambled ASO or Tau^{ASO-12} in the same treatment approach as for the 9- to 12-month-old cohort to determine whether survival could be extended, even in this older cohort ($n = 17$ per treatment). Mice were sacrificed when they could not flip over in 30 s. Despite this late treatment strategy, Tau^{ASO-12}–treated mice lived

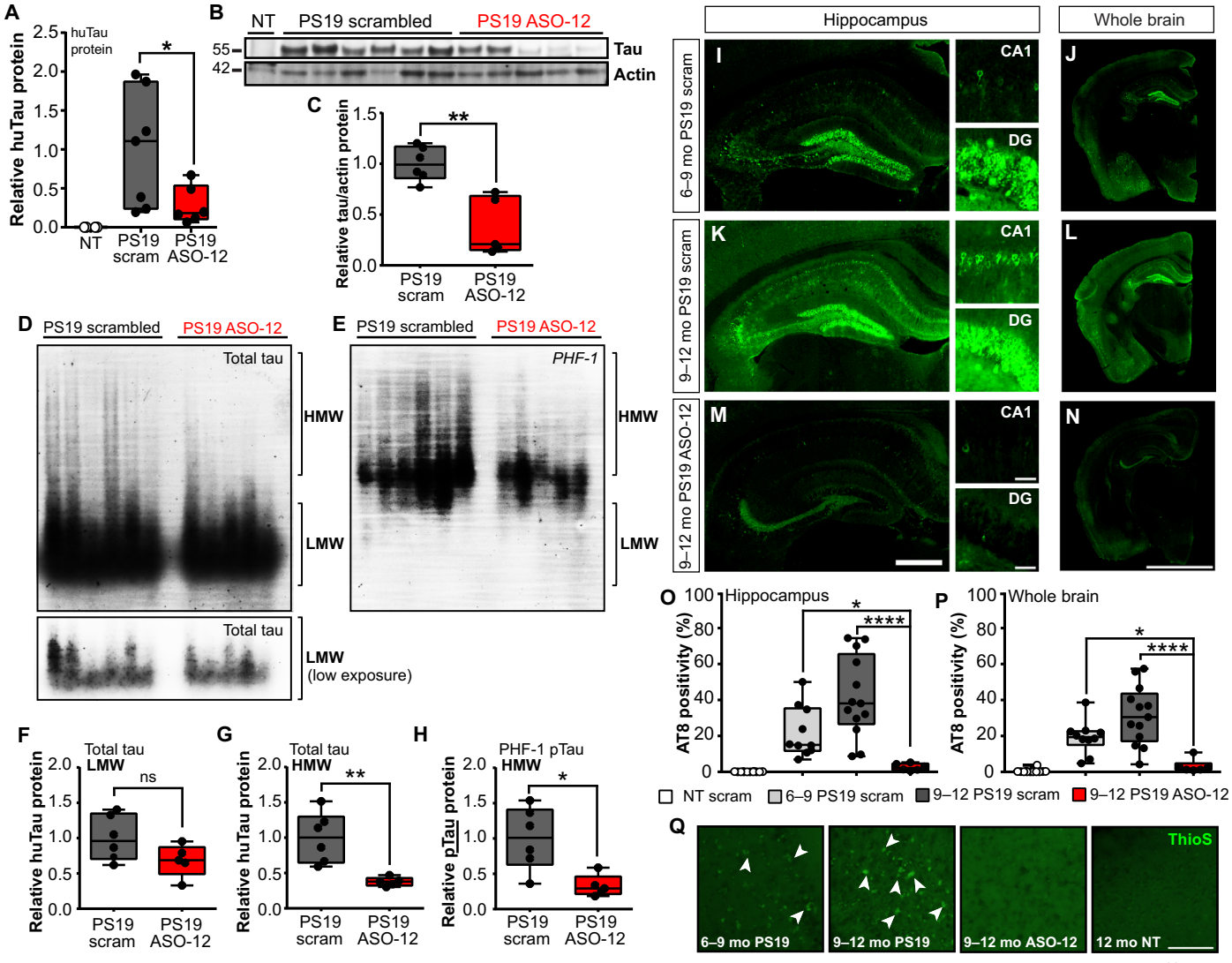

Fig. 2. Reducing human tau in aged Ps19 mice reverses tau pathology. (**A**) PS19 mice at 9 months of age were treated with scrambled ASO ($n = 6$) or Tau^{ASO-12} ($n = 6$) for 1 month at 30 μg/day. Scrambled ASO-treated nontransgenic mice served as control ($n = 5$). Alzet osmotic pumps were removed after 1 month, and mouse brain tissue was collected 2 months later. Total human tau protein was measured (one-way ANOVA, Sidak post hoc analysis). (**B** and **C**) Sarkosyl extraction was performed on mouse brain lysates and then run on Western blots and probed for total human tau (using antibody Tau13) and actin (B). Quantification of Western blots indicated less insoluble tau in PS19 mice treated with Tau^{ASO-12} compared to PS19 mice treated with scrambled ASO (C) (two-tailed Student's t test). (**D** and **E**) Mouse brain lysate was run on SDD-AGE and probed for total tau (D) and phosphorylated-tau (PHF-1; pS396/pS404) (E). (**F** to **H**) SDD-AGE HMW and low–molecular weight (LMW) bands were quantified in ImageJ (two-tailed Student's t test). pTau, phoshorylated tau. (**I** and **J**) Representative images of AT8 pathology in 9-month-old PS19 mice (pathology baseline). (**K** to **N**) Representative images of AT8 tau pathology in the mouse hippocampus and full-brain sections from 9- to 12-month-old PS19 mice treated with scrambled ASO or Tau^{ASO-12}. Scale bars, 500 μm (hippocampus panel), 50 μm (CA1, dentate gyrus), and 2.5 mm (whole brain). (**O** and **P**) Quantification of AT8-positive staining in the hippocampus (O) and whole brain (P) demonstrates a reversal in AT8 positivity in the Tau^{ASO-12}–treated PS19 9- to 12-month-old cohort compared to the 6- to 9-month-old scrambled ASO control group (one-way ANOVA, Sidak post hoc analysis). (**Q**) Representative images of Thioflavin S (ThioS) staining in the mouse piriform cortex showing reversal of Thioflavin S positivity in Tau^{ASO-12}–treated PS19 mice (quantification is shown in fig. S5). White arrowheads indicate neurons positive for NFTs. Scale bar, 100 μm. $^{*}P < 0.05$, $^{****}P < 0.0001$. Graphical data are represented as box and whisker plots with individual points overlaid, where error bars represent maximum and minimum values and the boxed line represents the median.

significantly longer than age-matched controls treated with scrambled ASO (Mantel-Cox survival, $P = 0.0052$; median survival: scrambled, 312 days; Tau^{ASO-12}, 348 days) (Fig. 5A).

In addition to survival, we assessed the ability of treated PS19 mice to complete a functional task. We sought to test the functionality of the mice and found nest building performance a robust and reliable readout of general performance in PS19 mice. In mouse models, instinctual nest building behavior is used to jointly assess general social behavior, cognitive performance, and motor capabilities. Deficits in nesting activity are evident in mouse models of tauopathy (*32*), suggesting that accumulation of tau can induce deficits in nesting practices. Mouse nesting deficits are characterized by incomplete nests (low nest score) and high untorn weight of the nestlet (3-g piece of pressed cotton). Eight- to 9-month-old PS19 mice were treated with

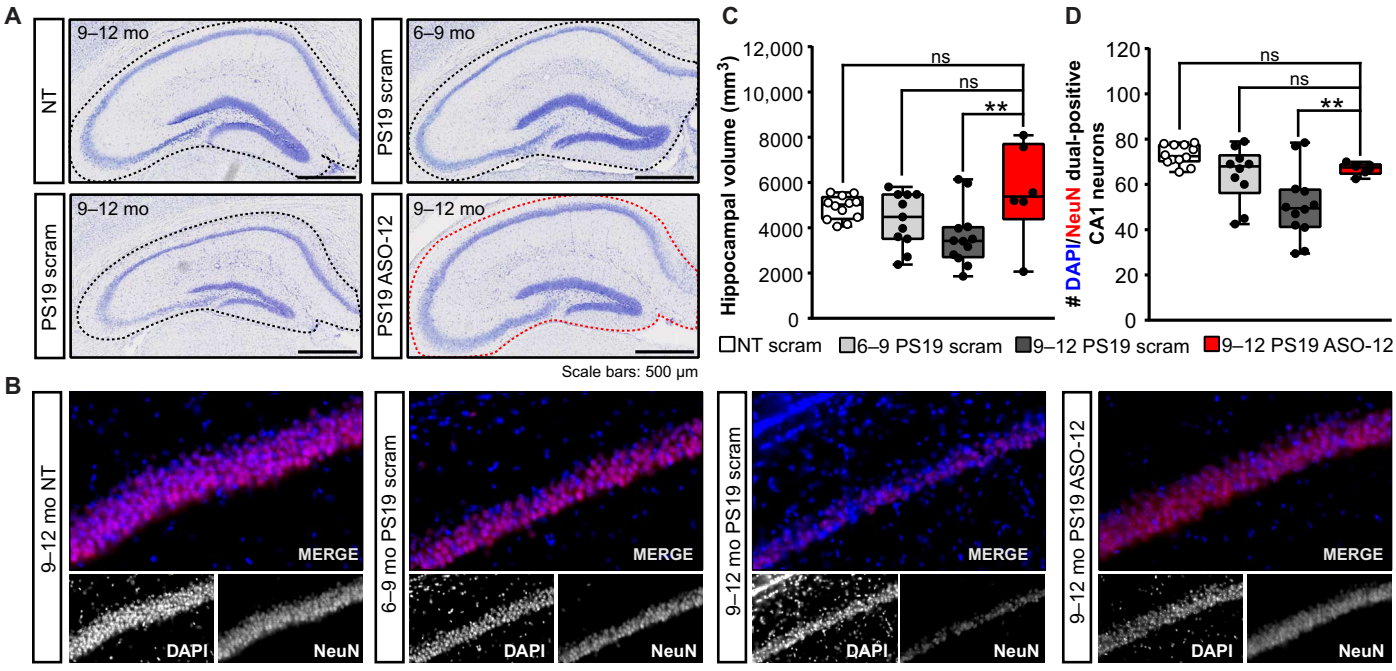

Fig. 3. Reducing human tau prevents hippocampal neuron loss in PS19 mice. (**A** and **C**) Brain sections systematically selected at 300-μm intervals throughout the hippocampus were taken from 9-month-old nontransgenic mice ($n = 6$), 12-month-old nontransgenic mice ($n = 6$), 9-month-old PS19 mice ($n = 10$), 9- to 12-month-old PS19 mice [both untreated ($n = 6$) and treated with scrambled ASO (n = 6)], and 9- to 12-month-old PS19 mice treated with Tau^{ASO-12} ($n = 6$). Representative images (A) and volume quantification (C) show hippocampal loss prevention in the Tau^{ASO-12} treatment group. (**B** and **D**) Representative images (B) and quantification (D) of the CA1 region of the hippocampus stained with the neuronal marker NeuN (red) and counterstained with the nuclear marker DAPI (blue) in a predefined CA1 region. Nine- to 12-month-old Tau^{ASO-12}–treated PS19 mice had more DAPI-positive neurons in CA1 than the age-matched PS19 controls treated with scrambled ASO (one-way ANOVA, Sidak post hoc analysis). *$P < 0.05$, **$P < 0.01$. Graphical data are represented as box and whisker plots with individual points overlaid, where error bars represent maximum and minimum values and the boxed line represents the median.

saline ($n = 11$), scrambled ASO ($n = 11$), or Tau^{ASO-12} ($n = 25$) at 30 μg/day for 4 weeks, and then the implanted Alzet osmotic pumps were removed. Six weeks after pump removal, nesting activity was assessed. No significant difference was seen between PS19 mice treated with saline and scrambled ASO, so these data were combined (nestlet weight: two-tailed Student's t test, $P = 0.366$; nestlet score: two-tailed Mann-Whitney U test, $P = 0.311$). Mice treated with Tau^{ASO-12} performed significantly better on the nestlet task, both making better nests ($P = 0.040$, Kruskal-Wallis, Dunn's post hoc analysis) and leaving less untorn nestlet weight behind ($P = 0.014$, one-way ANOVA, Sidak post hoc analysis) (Fig. 5, B and C). Functional deficits as depicted by survival and nesting activity in aged PS19 mice served as a practical alternative for traditional cognitive performance and could be rescued by reducing total human tau in vivo (Fig. 5, A to C).

Tau ASOs reduce tau in a nonhuman primate

Cynomolgus monkeys were treated with an ASO complementary to monkey tau. All monkeys were 2 to 8 years old at the start of treatment. Artificial CSF ($n = 4$)—a solution made to mimic the molecular composition of biological CSF—or the ASO was delivered in a single bolus via lumbar puncture into the intrathecal space at doses of 30 mg ($n = 3$) or 50 mg ($n = 3$), and the brains and spinal cords were collected 2 weeks later (Fig. 6A). Total tau mRNA was decreased across the spinal cord and brain in a dose-dependent manner (Fig. 6B). Next, we looked at tau mRNA and protein in the brain and spinal cord after both a short (2 weeks; $n = 4$ per treatment) and long (6 weeks; $n = 4$ per treatment) duration after initial dose. An initial intrathecal bolus of 10 mg of ASO was delivered, followed by a second 30 mg of ASO intrathecal bolus 1 week later (Fig. 6C). At 2 weeks after ASO treatment, tau mRNA was effectively decreased (Fig. 6D). Protein was also decreased, although not to the same degree, likely because of the long half-life of tau (Fig. 6E) (*33*). The longer 6-week duration showed both continued tau mRNA reduction and improved tau protein reduction compared to the 2-week duration (Fig. 6, D and E). Despite delivery of the ASO as a bolus in the intrathecal space, tau was suppressed just as efficiently in the entire hippocampus as it was in the cervical portion of the spinal cord, demonstrating widespread intrathecal delivery of ASO in the brain of a larger mammalian species.

Finally, we tested the effect of the ASO on tau protein in the CSF as a possible marker to monitor therapeutic efficacy (*34*). Nonhuman primates were given an ASO dose of 10 mg via intrathecal bolus injection, followed by a 30 mg of ASO bolus 1 week later. Brains and spinal cords were collected 5 weeks after the initial dose. Tau protein in the CSF was measured both before dosing and at necropsy (Fig. 6F) ($n = 4$ per treatment). Tau protein reduction in the spinal cord and in the frontal cortex, temporal cortex, and hippocampus was confirmed (Fig. 6G). Using the individual animal's predosing CSF tau as a baseline, tau protein in the CSF was found to be decreased after tau ASO treatment (Fig. 6H). CSF tau correlated directly with tau protein in the hippocampus ($P = 0.01$, $R^2 = 0.68$, linear regression; Fig. 6J; for other regions, see fig. S9), one of the major affected regions in the AD brain.

DISCUSSION

Using ASOs specifically directed against human tau in the PS19 tauopathy mouse model at 6 and 9 months of age, we found a marked

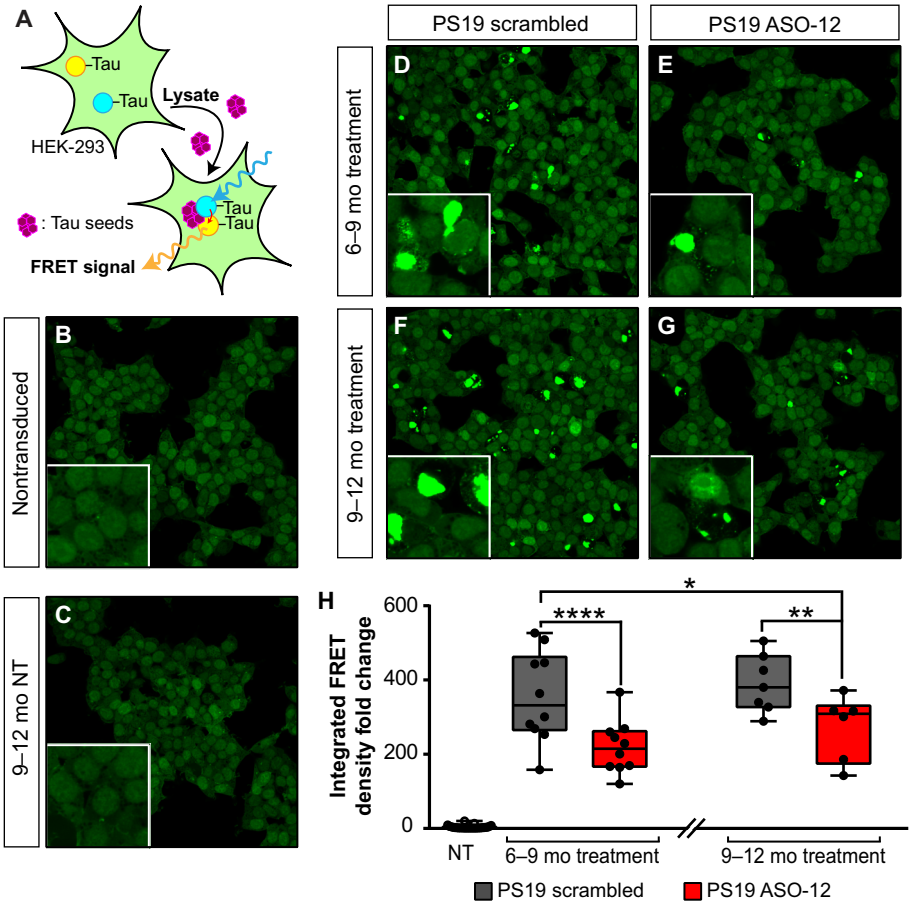

Fig. 4. Tau seeding activity is reversed after human tau reduction. (**A**) Schematic of the in vitro FRET tau seeding assay. (**B** and **C**) Representative images of HEK-293 Tau^{RD}-CFP/Tau^{RD}-YFP sensor cells not treated with mouse brain lysate (B) or treated with brain lysate from 9- to 12-month-old nontransgenic mice (C). (**D** to **G**) Representative confocal FRET images of sensor cells treated with brain lysates from 6- to 9-month-old (D and E) or 9- to 12-month-old (F and G) PS19 mice treated with scrambled ASO or $Tau^{ASO\text{-}12}$. Tau aggregation was visible in all conditions as was evident by the accumulation of FRET-positive inclusions detected with confocal microscopy, but was reduced in sensor cells exposed to brain lysates from $Tau^{ASO\text{-}12}$–treated mice in both the 6- to 9-month-old and 9- to 12-month-old age groups. (**H**) Normalized integrated FRET density (the percent of FRET-positive cells multiplied by the median fluorescence intensity of those FRET-positive cells and normalized to cells not treated with brain lysate) fold change in quantitative "tau seeding" values for all samples. Tau seeding activity was reduced in brain lysates from both the 6- to 9-month-old and 9- to 12-month-old PS19 $Tau^{ASO\text{-}12}$–treated mice compared to age-matched PS19 scrambled ASO-treated mouse brain lysates. Tau seeding activity in the 9- to 12-month-old $Tau^{ASO\text{-}12}$–treated brain lysates was reversed when compared to the younger 6- to 9-month-old scrambled ASO-treated control mouse brain lysates (one-way ANOVA, Sidak post hoc analysis). $^{*}P < 0.05$, $^{**}P < 0.01$, $^{***}P < 0.001$, $^{****}P < 0.0001$. Graphical data are represented as box and whisker plots with individual points overlaid, where error bars represent maximum and minimum values and the boxed line represents the median.

decrease and even reversal of phosphorylated AT8 tau pathology across the brain despite the age at treatment (Figs. 1 and 2). Tau knockdown treatment also halted hippocampal and neuronal loss (Fig. 3), reversed tau seeding activity (Fig. 4), and protected against deficits in survival and nesting behavior (Fig. 5). When tested in nonhuman primates, tau ASOs targeting monkey tau were highly efficacious at reducing endogenous tau mRNA and protein throughout the brain, spinal cord, and CSF after intrathecal dosing (Fig. 6). When combined, these data support the use of a tau-lowering therapy for human patients with tauopathies.

Previous studies have similarly identified reductions and even reversal of pathological tau lesions (*35*) and memory improvement (*36*) through suppression of the mutant tau gene by doxycycline administration in Tg4510 mice. Despite their overall less severe phenotype compared to the Tg4510 model, PS19 mice do develop Thioflavin S positivity and NFT pathology in the brain (*22*), consistent with tau deposition seen in postmortem human brain tissue. The reversal of tau pathology by ASO-mediated reduction of human tau in PS19 mice not only is consistent with previous studies using a regulated transgene but also shows the therapeutic potential for tau-targeted strategies by demonstrating reduction in tau seeding activity and rescue of neuronal loss in a clinically relevant tauopathy mouse model. Despite there being more tau aggregates in the 9- to 12-month-old treated PS19 cohort compared to the 6- to 9-month-old animals, seeding activity was reduced equally in both groups. We do not know whether this represents biological variability or reflects underlying important biology, suggesting that ASOs have an overall greater impact on seeding at the later 9- to 12-month time point. Although tau pathology can still be measured, unfortunately, a less severe tauopathy mouse model limits complete assessment of behavioral outcomes, because others have failed to see significant differences in some of these more classic cognitive tests, such as the Morris water maze and contextual fear behavior (*37*, *38*). Despite the absence of changes in cognition on traditional tests, PS19 mice demonstrated functional decline evident in nesting activity deficits and premature death, which were both prevented by tau-lowering ASO treatment.

A major question in developing therapeutics for symptomatic neurodegenerative disease is whether the disease can be substantially slowed or even improved once the degenerative disease process has already begun. By the time most patients with tauopathy come to the clinic with symptoms, tau inclusions most likely have already begun to be deposited. Several reports describe using genetic tools to reverse neurodegeneration in animal models (*17*, *39*). With our readily translatable human ASO therapeutic, we were able to reverse pathological changes and prevent neuronal loss, improve behavioral deficits, and extend survival in PS19 mice. The fact that pathology reversal can be achieved should perhaps not be too surprising. Dominantly inherited forms of neurodegenerative diseases caused by mutations in tau, SOD1, huntingtin, or other proteins are all highly age-dependent, suggesting that mechanisms early in life may adequately mitigate the effects of these disease-causing mutant proteins and delay disease onset.

By definition, primary tauopathies include those with disease-causing mutations in tau in addition to progressive supranuclear palsy (PSP), corticobasal degeneration, and Pick's disease. However, genetic

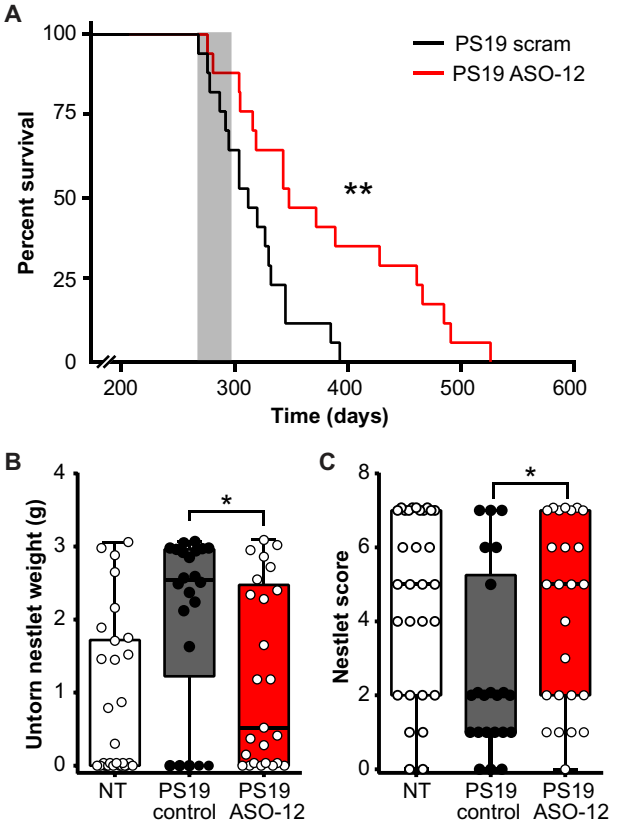

Fig. 5. Human tau reduction extends PS19 mouse survival and prevents nesting behavioral deficits. (**A**) Nine-month-old PS19 mice were treated with scrambled ASO or $Tau^{ASO\text{-}12}$ (n = 17 per treatment) for 1 month at 30 μg/day (gray bar), and survival was monitored. $Tau^{ASO\text{-}12}$ treatment prolonged survival (median survival, 348 days) compared to scrambled ASO control treatment (median survival, 312 days) [log-rank (Mantel-Cox) test]. (**B**) PS19 mice at 8 to 9 months of age were treated with saline (n = 11), scrambled ASO (n = 11), or $Tau^{ASO\text{-}12}$ (n = 25) for 1 month at 30 μg/day. Treatment of nontransgenic mice with scrambled ASO (30 μg/day) served as the control (n = 30). Alzet osmotic pumps were removed after 1 month, and nestlets were provided to the mice 6 weeks later. PS19 mice treated with saline or scrambled ASO showed no significant difference in untorn nestlet weight or nestlet score, and thus these data were combined (control). A perfect nest will have no untorn nestlet left and will weigh less, whereas a poor nest will have more untorn nestlets that will weigh more. PS19 mice treated with $Tau^{ASO\text{-}12}$ had significantly less untorn nestlet material than control-treated PS19 mice (one-way ANOVA, Sidak post hoc analysis). (**C**) Nestlet score was blindly measured on a scale from 0 (untouched nestlet) to 7 (perfect nest). PS19 mice treated with $Tau^{ASO\text{-}12}$ constructed better nests than did control PS19 mice (Kruskal-Wallis test, Dunn's post hoc analysis). *P < 0.05. Graphical data are represented as box and whisker plots with individual points overlaid, where error bars represent maximum and minimum values and the boxed line represents the median.

tau data for PSP suggest that tau is, at least partially, causative in these disorders rather than solely a pathological hallmark (*40*). With recent advances in PSP human clinical trials, lowering tau in PSP would be an excellent application of this tau ASO strategy (*41*, *42*). Further, in about 40% of FTD cases, tau is the primary pathology (*43*). Although still in the early characterization stages, we anticipate that tau positron emission tomography (PET) ligands will, in the near future, help distinguish FTD with tau from other FTD cases and thus enable a tau-focused therapeutic trial in the FTD patient population (*44*). In addition to a primary tauopathy diagnosis and tau PET imaging, genetic tests could be used to identify patients with a tau mutation, or the H1 tau haplotype (*45*), or tau-specific single-nucleotide polymorphisms that increase tau expression (*46*, *47*), or other genetic polymorphisms such as the rs1768208 T-allele (*48*) or PIN1 (*49*), which are linked to greater tau deposition, as a possible means to determine who may qualify for a tau-lowering treatment.

Although several different primary tauopathy disorders exist, including PSP and FTD, the most common tauopathy is AD. In AD, tau burden appears to directly correlate with disease progression and cognitive decline (*3*). However, one of the major issues in considering treating AD with a tau-modifying therapy is the ongoing deposition of β-amyloid (Aβ). Some data suggest that Aβ toxicity is partially mediated through tau (*50*–*52*) as the tau knockout mouse has proven to be protected against a growing number of Aβ-induced insults, including those affecting cognition (*50*, *53*), seizures (*14*, *50*, *51*, *54*, *55*), survival (*50*, *51*, *54*), axonal transport (*52*), and double-stranded breaks in DNA (*55*). Thus, there is still potential for treating AD with a human tau ASO therapy. One of the surprising findings when looking at the effects of tau reduction in mouse models of Aβ deposition was the importance of tau in neuronal hyperexcitability. Our previous work emphasized this point by demonstrating that lowering tau in adult mice with a tau ASO was also protective against seizures (*15*). Although traditional oral antiepileptic drugs will remain the mainstay for treating most seizure disorders, for some epilepsies with poor responses to these medications, lowering tau may be a viable consideration.

Another key consideration for testing tau-lowering therapy in human clinical trials will be the safety of reducing total levels of tau because tau is an abundant and likely important protein in the nervous system. Surprisingly, mice that completely lack tau have proven to be phenotypically normal in terms of learning/memory and general cognition (*13*, *14*, *50*) with a minor motor phenotype developing later in life, the severity of which varies (*12*–*14*, *56*). When endogenous murine tau is reduced in adult mice, no deviations from baseline are seen in any sensory, motor, or cognitive behavior task (*15*), adding support to the safety of reducing tau in the adult mammalian brain. Given that tau ASOs also effectively reduce monkey tau (Fig. 6), important toxicology work can now be carried out to determine the safety of reducing tau in nonhuman primates to help further assess the risks of tau lowering in humans. Future preclinical studies would also benefit from measurements of tau and phosphorylated tau in the CSF following ASO-mediated tau reduction because these assessments are already being used as markers of disease in human patients.

It is important to note the limitations associated with this study. Although we predict that lowering tau with ASOs in any tauopathy model would show similar benefit, our study here was restricted to the PS19 mouse model of tauopathy (*22*). To achieve rapid pathology in mice, the tau transgene is both mutated with a Tau^{P301S} point mutation and expressed at high levels. Thus, it is possible that some of the effects seen here are associated with artificially high expression of a mutant form of tau, an important caveat when considering treating those AD patients who have neither a tau mutation nor tau overexpression. In addition, correlating behavioral changes in mice with cognitive deficits in humans is challenging, and it remains unclear how the benefits we observed here will translate to humans. Last, although previous ASO studies in humans are encouraging, the ASOs used here need to be fully tested in formal toxicology studies before they can advance toward human clinical trials.

The preclinical tau reduction work presented here, in conjunction with our previous murine tau ASO data (*15*), sets the stage for translating a tau ASO program into the clinic. A similar ASO strategy targeting

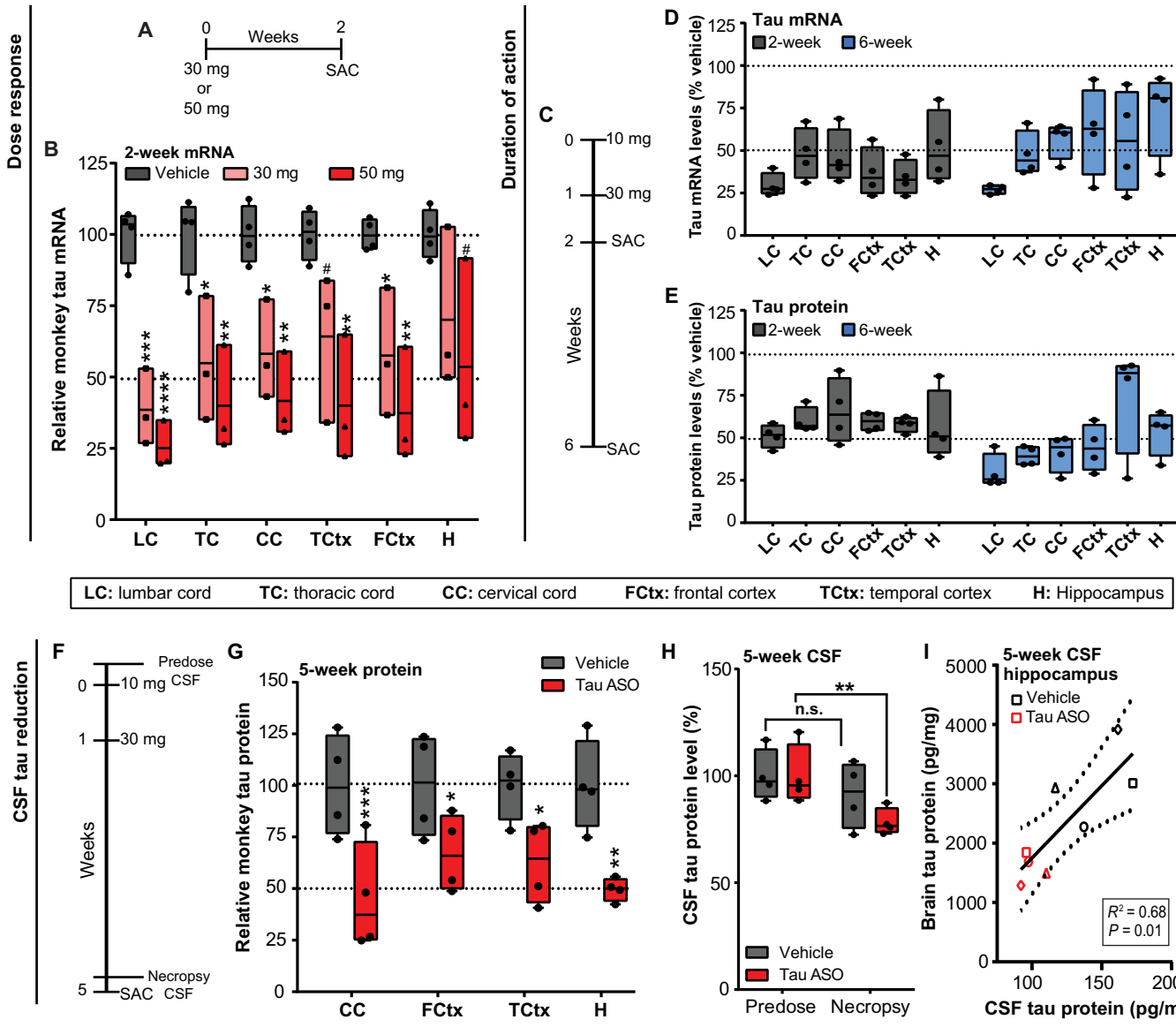

Fig. 6. Tau ASOs reduce tau protein in the nonhuman primate brain and CSF. (**A**) Experimental design for 2-week dosing study. SAC, sacrifice. (**B**) Quantification of total endogenous tau mRNA in the spinal cord and brain of cynomolgus monkeys after ASO treatment. Data are expressed as percent vehicle (artificial CSF). Nonhuman primates received a single dose via lumbar puncture of either vehicle ($n = 4$), 30 mg ($n = 3$), or 50 mg ($n = 3$) ASO against monkey tau. Tissue was collected 2 weeks after the single-dose treatment (one-way ANOVA, Sidak post hoc analysis). (**C**) Experimental design for 6-week duration of action study. Nonhuman primates were given tau ASO at a dose of 10 mg followed by a repeat dose of 30 mg of tau ASO 1 week later. Control monkeys were treated with vehicle for both injections. Tissue from half of the monkeys was collected at 2 weeks after treatment (control, $n = 4$; tau ASO, $n = 4$), and tissue from the remaining monkeys was collected at 6 weeks after the initial dose (control, $n = 4$; tau ASO, $n = 4$). (**D** and **E**) Total tau mRNA (D) and protein (E) were measured in spinal cord and brain regions at 2 and 6 weeks after initial dose. (**F**) Experimental design for 5-week brain and CSF tau protein analysis. (**G**) Quantification of total endogenous tau protein in the spinal cord and brain of nonhuman primates 5 weeks after the initial dose of ASO or vehicle (control, $n = 4$; tau ASO, $n = 4$) (one-way ANOVA, Sidak post hoc analysis). (**H**) CSF was drawn just before the initial dose and again just before necropsy. The percent change in total tau in the CSF between the two time points for each treatment group was calculated (two-way repeated-measures ANOVA, Sidak post hoc analysis). (**I**) CSF tau protein directly correlated with the total tau protein in the hippocampus (linear regression). $^{\#}P < 0.01$, $^{*}P < 0.05$, $^{**}P < 0.01$, $^{***}P < 0.001$, $^{****}P < 0.0001$. Graphical data are represented as box and whisker plots with individual points overlaid, where error bars represent maximum and minimum values and the boxed line represents the median.

SOD1 resulted in extended survival in a rat model of ALS (*16*). A recently completed phase 1 clinical trial in human ALS patients demonstrated that CSF delivery of human SOD1 ASOs had an excellent safety profile (*21*); a subsequent phase 1/2 clinical trial is now underway (ClinicalTrials.gov; #NCY02623699). Further, ASOs against the mutant survival motor neuron mRNA that rescued rodent models of spinal muscular atrophy (SMA) (*57*) just completed phase 3 studies for children with SMA and have been approved by the U.S. Food and Drug Administration (*58*). ASOs against mutant human huntingtin that successfully treated mouse models of Huntington's disease (*17*) are now in human clinical trials as well. These in vivo preclinical and early clinical ASO studies, together with the preclinical data presented here, strengthen the case for a human tau reduction therapeutic approach for patients with PSP, FTD, AD, and other tauopathies.

MATERIALS AND METHODS

Study design

The goals of the study were to treat adult PS19 mice with a human tau–lowering ASO and analyze the effects of tau reduction on tau pathology, inflammation, neuronal loss, tau seeding, and functional behavior. The first portion of the study focused on treatment with $Tau^{ASO\text{-}12}$ directed against human tau and used PS19 mice—a tauopathy mouse model that overexpresses a mutant form of human tau—and their nontransgenic littermate controls. For all studies, mice were litter-matched, age-matched, and gender-matched to keep the treatment groups as similar as possible. Except for the duration of action study where the mice were euthanized at different time points, all studies were predetermined to last 3 months from pump implantation. Each age group—6- to 9-month-old and 9- to 12-month-old—was processed together, and all brains across both age groups were stained and imaged at the same time. The tau seeding assay was carried out in HEK-293 cells that stably expressed the Tau^{RD} fused with CFP and Tau^{RD} fused with YFP (*30*). Sample sizes were chosen on the basis of both previous experience with tau ASOs in the laboratory and therapeutic studies carried out by others using the same PS19 mouse line. The tau seeding analyses, quantification of AT8 staining, hippocampal and entorhinal volume, NeuN/DAPI counts, cell size analysis, survival, and nestlet behavior were all carried out blinded. The last part of the study used cynomolgus nonhuman primates (total of $n = 34$) to determine the extent of tau mRNA and protein reduction after a lumbar infusion of tau ASO in a large mammal.

Animals

The PS19 mice were created using a 1N4R tau complementary DNA with a Tau^{P301S} mutation resulting in fivefold greater human tau expression over endogenous mouse tau (*22*). Breeding pairs were purchased from The Jackson Laboratory, and resulting progenies were maintained on a B6C3 background. All nontransgenics used were littermates of PS19 mice. All studies were performed using gender-balanced groups. Mice had access to food and water ad libitum and were housed on a 12-hour light/dark cycle. Experiments involving animals were approved by the Animal Studies Committee at Washington University in St. Louis.

Antisense oligonucleotides

The ASOs used have the following modifications: 5 nucleotides on the 5′ and 3′ termini containing 2′-*O*-methoxyethyl modifications, 10 unmodified central oligodeoxynucleotides to support RNase H activity, and a phosphorothioate backbone to improve nuclease resistance and promote cellular uptake (*59*). ASOs were synthesized as previously described (*60*) and solubilized in 0.9% sterile saline immediately before use. For murine use, the sequences were as follows: $Tau^{ASO\text{-}12}$, 5′-GCTTTTACTGACCATGCGAG-3′; scrambled, 5′-CCTTCCCTGAAGGTTCCTCC-3′. For nonhuman primate work, the sequence was as follows: tau ASO sequence, 5′-CCGTTTTCTTACCACCCT-3′.

Surgical placement of ICV pumps and tissue collection

As previously described (*16*, *61*), mice were anesthetized with isoflurane, and 28-day Alzet osmotic pumps with ASO were implanted in a subcutaneous pocket formed on the back of the mice. The catheter was placed in the right lateral ventricle with the following coordinates based on bregma: −0.5 mm posterior, −1.1 mm lateral (right), and −2.5 mm ventral. For tissue collection, mice were anesthetized with isoflurane and perfused using chilled phosphate-buffered saline (PBS)–heparin. Brain tissue was rapidly removed, and the right hemisphere (ipsilateral to the pump catheter placement) was snap-frozen in liquid nitrogen and stored at −80°C, whereas the left hemisphere (contralateral to the catheter placement) was postfixed in 4% paraformaldehyde at 4°C and transferred to 30% sucrose 24 hours later. All animal protocols were approved by the Washington University in St. Louis Institutional Animal Care and Use Committee.

Quantitative real-time polymerase chain reaction

RNA analyses were performed using quantitative real-time polymerase chain reaction (qRT-PCR). Total RNA was extracted from brain tissue using a Qiagen RNeasy Kit (Qiagen). For total tau analyses, RNA was reverse-transcribed and amplified using the EXPRESS One-Step Superscript qRT-PCR Universal Kit (Invitrogen). The qRT-PCRs were run and analyzed on the ABI PRISM 7500 Fast Real-Time PCR System (Applied Biosystems). Total human and mouse tau expression levels were normalized to mouse glyceraldehyde-3-phosphate dehydrogenase (GAPDH) mRNA levels and analyzed using the $\Delta\Delta^{Ct}$ method for relative expression analysis. Primer/probe sequences were as follows: human total tau, 5′-AGAAGCAGGCATTGGAGAC-3′ (forward), 5′-TCTTCGTTTTACCATCAGCC-3′ (reverse), and 5′-/56-FAM/ACGGGACTGGAAGCGATGACAAAA/3IABkFQ/-3′ (probe); mouse total tau, 5′-GAACCACCAAAATCCGGAGA-3′ (forward), 5′-CTCTTACTAGCTGATGGTGAC-3′ (reverse), and 5′-/56-FAM/CCAAGAAGGTGGCAGTGGTCC/3IABkFQ/-3′ (probe); GAPDH: 5′-TGCCCCCATGTTGTGATG-3′ (forward), 3′-TGTGGTCATGAGCCCTTCC-3′ (reverse), and 5′-/56-FAM/AATGCATCCTGCACCACCAACTGCTT/3IABkFQ/-3′ (probe) (Integrated DNA Technologies).

Tau ELISA analysis

Tissues were homogenized in RAB buffer [100 mM MES, 1 mM EDTA, 0.5 mM $MgSO_4$, 750 mM NaCl, 20 mM NaF, and 1 mM Na_3VO_4, supplemented with protease inhibitor (cOmplete, Roche)]. Homogenate was spun at 40,000*g* on an ultracentrifuge for 20 min at 4°C. Supernatant was collected, and protein concentration was measured using Pierce Bicinchoninic Acid (BCA) Protein Assay Kit (Thermo Scientific). Total human tau protein levels were measured on a Tau5-HT7 sandwich enzyme-linked immunosorbent assay (ELISA). Ninety-six–half–well plates (Nunc) were coated with the Tau-5 antibody (anti-mouse; Millipore) overnight at 4°C. Plates were blocked with 4% bovine serum albumin (BSA) for 60 min at 37°C, and brain homogenate diluted in standard buffer (0.25% BSA, 300 mM tris, 0.05% azide, and 1× protease inhibitor in PBS) was added and incubated overnight at 4°C. For the standard curve, hTau2N4R recombinant protein was used. The detection antibody biotinylated HT7 (anti-mouse; Thermo Scientific) was added the next day followed by streptavidin poly–horseradish peroxidase–40 (Fitzgerald). Plates were developed using Super Slow ELISA TMB (Sigma-Aldrich) and read on an Epoch Microplate Spectrophotometer (BioTek).

Sarkosyl-insoluble tau analysis

The sarkosyl extraction was carried out as previously described (*62*). Briefly, tissue was homogenized in buffer H [20 mM tris-HCl (pH 7.5), 0.15 M NaCl, 1 mM EGTA, 1 mM dithiothreitol] with electronic handheld homogenizer and then spun at 100,000*g* for 30 min at 4°C in the ultracentrifuge. Supernatant was removed, pellet was resuspended in buffer H, and homogenized again. Samples were then incubated with 1% Triton X-100 at 37°C for 30 min. Samples were spun at 100,000*g* for 30 min at 4°C, and supernatant was removed. Pellet was resuspended in buffer H and homogenized. Samples were then incubated with 1% sarkosyl at 37°C for 30 min. After the

incubation, samples were spun at 100,000*g* for 30 min at 4°C. Supernatant was removed and stored as the sarkosyl-soluble fraction. The pellet was resuspended in urea buffer [8 M urea, 50 mM tris-HCl (pH 7.5)] and sonicated. Samples were again spun at 100,000*g* for 30 min at 4°C. This supernatant was collected and used as the sarkosyl-insoluble fraction. Protein concentration was measured on BCA (Pierce). Five micrograms of sarkosyl-insoluble fraction and 6 μg of Triton X–soluble fraction were loaded onto a 4 to 20% SDS–polyacrylamide gel electrophoresis gel and transferred to polyvinylidene difluoride (PVDF) membrane. Tau13 (anti-mouse; 1:1000; Abcam) was used to detect total human tau on the sarkosyl-insoluble blot, and actin (anti-mouse; 1:2000; Abcam) was used on the Triton X–soluble blot as a loading control. Primary antibody was incubated at room temperature with 1:1 Odyssey blocking buffer/water for 3 hours. Membranes were washed three times with tris-buffered saline (TBS)–Tween, probed with goat anti-mouse IRDye 800 (1:2000, LI-COR) for 1.5 hours at room temperature, washed three times in TBS-Tween, and developed on the Odyssey CLx Imager (LI-COR). Bands were quantified using ImageJ software.

Semidenaturing detergent agarose gel electrophoresis

The SDD-AGE protocol was carried out as previously described (*63*) with minor modifications. Brain protein used for SDD-AGE analysis was collected by dounce homogenizing tissue in 1× PBS supplemented with protease inhibitor and spun at 3000*g* for 5 min at 4°C. The supernatant was collected, and protein concentration was measured by BCA (Pierce). The gel was composed of 1.5% agarose dissolved in buffer G (20 mM tris-base and 200 mM glycine), and 0.02% SDS added after the agarose was fully dissolved. Gels were cast to be 20 cm long. Fifty micrograms of total lysate was then incubated with 0.02% SDS sample buffer for 7 min at room temperature immediately before loading. Once loaded, the SDD-AGE was run using Laemmli buffer (buffer G + 0.1% SDS) at 30 V for 16 hours. The transfer was performed with capillary action using 20 pieces of thick Whatman paper (GB 005) and 8 pieces of medium high absorbent Whatman paper (GB 003) to Immobilon PVDF (Millipore) membrane at 4°C for 24 hours using 1× TBS. After transfer, the membrane was blocked in Odyssey Blocking Buffer PBS (LI-COR) for 1 hour and then probed for both total tau (anti-rabbit; 1:4000; Abcam) and PHF-1 (anti-mouse; 1:5000; gift from P. Davies) overnight at 4°C in 1:1 Odyssey blocking buffer/water. The membrane was washed three times with TBS-Tween, probed with goat anti-rabbit IRDye 680 (1:2000, LI-COR) and goat anti-mouse IRDye 800 (1:2000; LI-COR) for 1.5 hours at room temperature, washed three times in TBS-Tween, and developed on the Odyssey CLx Imager (LI-COR). To quantify the bands, we quantified the LMW and HMW portions of the blot separately. Previous reports of HMW and LMW tau run on SDD-AGE show an accumulation of LMW tau at the bottom of the gel with smears of HMW tau oligomers at the top (*7*, *63*–*65*). Using ImageJ gel quantification tool, each region—either HMW or LMW—was outlined and plotted. The middle empty lane was used to subtract background from all samples.

Immunofluorescence

Brains postfixed in 4% paraformaldehyde were sliced at 50 μm on a freezing microtome. Brains were incubated with the primary antibodies Pan-ASO (anti-rabbit; 1:2000; Ionis), AT8 (anti-mouse; 1:500; Thermo Scientific), NeuN (anti-rabbit; 1:100; Abcam), or GFAP (anti-chicken; 1:1000; Abcam) in 3% Horse Serum 1× TBS 0.1% Triton overnight at 4°C, followed by a 1-hour incubation at room temperature with fluorescent-conjugated secondary antibodies (1:400 anti-mouse DyLight 488 and 1:400 anti-rabbit DyLight 550, ThermoScientific). All sections were counterstained with DAPI for 5 min immediately after secondary incubation, mounted onto slides, and coverslipped using Vectashield mounting solution (Vector Labs). Fluorescent images were captured using the Olympus Nanozoomer 2.0-HT (Hamamatsu) and processed using the NDP viewer software (Hamamatsu). All images were taken with the same fluorescent settings and subsequently adjusted equally for brightness and contrast to ensure accurate pathology quantification.

Thioflavin S staining

Four brain sections 300 μm apart were used from each mouse. Staining for all sections analyzed was carried out on the same day and imaged together to reduce staining batch variability. Fifty-micrometer fixed brain sections were mounted onto slides and dried overnight. Slides were then incubated with fresh/filtered 0.05% Thioflavin S in 50% ethanol for 8 min in the dark, followed by dipping in 80% ethanol for 15 s. Slides were washed in double-distilled water five times for 5 min each in the dark. Sections were coverslipped with Vectashield mounting medium with propidium iodide (Vector Labs) and sealed with nail polish. Images were obtained using the 488 channel on an Olympus BX51 microscope mounted with a DP 70 Olympus digital camera. The number of Thioflavin S–positive cells was counted in the piriform cortex of each section and averaged together over the four sections for each mouse, resulting in one value per mouse.

Tau pathology quantification

All pathology quantification was carried out blinded. For AT8 pathology staining, four brain sections 300 μm apart were used from each mouse. Staining for all sections analyzed was carried out on the same day and imaged together to reduce staining batch variability. The sections were used to assess the percent area covered by AT8-positive tau staining. After imaging, using sections incubated only with secondary antibody, the brightness and contrast were adjusted using the NDP viewer software (Hamamatsu) to eliminate background, so the AT8-positive signal could be seen more clearly. Those exact same settings were then applied to all subsequent image files before being exported and saved as .jpeg image files. The image files were opened in ImageJ, converted to 8-bit grayscale, and resaved. Using the freehand selection tool on the grayscale images, the outline of either the whole-brain section or the hippocampus was drawn. A uniform threshold value of 6 (using the dark background option) was then applied before performing the "analyze particles" task to determine within the outline area the percent covered by positive signal. The average percent coverage of all four sections was used as the final percent AT8 stained value for that mouse.

Hippocampal volume and entorhinal cortex analysis

All hippocampal volume and entorhinal cortex analyses were carried out blinded. Starting at the very beginning of the hippocampus (bregma, −1.0 mm), eight sections were taken at 300 μm apart. Sections were mounted and stained with crystal violet before imaging on the Olympus Nanozoomer 2.0-HT (Hamamatsu). Using the NDP viewer software, the hippocampus in each section was outlined to obtain the total hippocampal area. Each of the hippocampal areas was then multiplied by 300 μm to obtain a final hippocampal volume in cubic millimeter for each mouse. For the entorhinal cortex, only sections posterior of bregma −2.70 mm were used. The entire cortex area ventral to the rhinal fissure

was outlined, and area was measured. This area was averaged across sections to obtain a final entorhinal/piriform area.

DAPI count and cell size analysis

For DAPI counts, a rectangle was placed over CA1 in ImageJ. Using a macro, the same-size rectangle was used for each section to ensure the same area. The numbers of DAPI-positive nuclei that colocalized with the NeuN neuronal marker were blindly counted within the defined CA1 region. For cell size analysis, three sections per mouse were subjected to crystal violet staining and imaged using the Olympus Nanozoomer 2.0-HT (Hamamatsu). To measure cell size area, 25 adjoining cells in CA1 spanning an average of 100 μm (about 8% of the total length of CA1) of the hippocampus in each section were outlined using the NDP viewer software at a magnification of ×40, and the area of each of those cells was measured. The cell size area of those 25 cells was averaged for each section, and those averages for the three sections were then averaged for each mouse, generating a single cell size area value for each animal.

Tau seeding assay

In vitro tau seeding activity was measured as previously described (*30*, *31*). Briefly, HEK-293 cells stably expressing the repeat domain of tau with the P301S mutation (TauRD^{P301S}) fused with CFP and TauRD^{P301S}-YFP were plated in 96-well plates at 35,000 cells per well. About 18 hours later, at 60% confluency, cells were transduced with the experimental PS19 brain lysate at 4 μg per well. The transduction complexes were generated by incubating Opti–minimum essential medium (MEM) (Gibco) + 4-μg lysate with Opti-MEM + 1.25-μl Lipofectamine 2000 (Invitrogen) for a final volume of 20 μl per well for 20 min at room temperature. Transduction complexes were added to cells for 24 hours, and then cells were harvested with 0.05% trypsin followed by postfixing in 2% paraformaldehyde (Electron Microscopy Sciences) for 10 min. Cells were then resuspended in flow cytometry buffer. For all flow cytometry measurements, the MACSQuant (Miltenyi) flow cytometer was used. CFP and FRET were measured by exciting cells with the 405-nm laser and capturing fluorescence with the 405-/50- and 525-/50-nm filters, respectively. For FRET quantification, a bivariate plot of FRET versus CFP was generated to assess the number of FRET-positive cells, using cells that received Lipofectamine alone as a marker of the FRET-negative population. The integrated FRET density (percentage of FRET-positive cells multiplied by the median fluorescence intensity of FRET-positive cells) was used for all quantitative analyses. Each experiment was performed using 20,000 cells per replicate, and each sample was analyzed in triplicate. Data analyses were performed with FlowJo v10 (Tree Star). Representative images of tau aggregates in the HEK dual-positive cells were taken using a confocal microscope with the BP (band pass) 505-530 filter.

Survival analysis

Nine-month-old PS19 mice were treated with either scrambled ASO or Tau^{ASO-12} at 30 μg/day for 28 days. Immediately after pump implantation, animals were monitored several days a week throughout the study. If a mouse showed signs of hindlimb paralysis, then it was tested daily for its ability to right itself when placed on its back. Mice unable to flip over after 30 s were sacrificed.

Nestlet behavior

To measure nesting capability, singly housed PS19 mice were given an intact, preweighed compressed cotton nestlet (3.0 g; Ancare) in their cage. After 24 hours, images were taken for each nest, and any untorn nestlets were removed, dried overnight at 37°C, and weighed. Nest quality was scored on a scale of 0 to 7, with slight modifications and increased scale range compared to previously published criteria (*66*). A score of 7 is a perfect nest with no untorn nestlet remaining, whereas a score of 0 is an untouched nestlet. The untorn nestlets were weighed, and nests were scored by a blinded observer.

Nonhuman primate ASO dosing

All nonhuman primate procedures were performed following animal welfare regulations of the institution. All nonhuman primates were 2 to 8 years old at the start of treatment. Intrathecal lumbar bolus injections were performed in cynomolgus monkeys after anesthesia with ketamine and domitor (antisedan used as an antidote). Ten-, 30-, and 50-mg doses of tau ASO were administered via lumbar puncture at level L3-L4 and infused over the course of 1 min as a slow bolus. At the discretion of the study veterinarian, some doses were administered at the L5-L6 level as an alternative when the intrathecal space was not accessible at L3-L4. Neurological exams were performed after dosing and then again before necropsy. The spinal cord and brain were collected either 2, 5, or 6 weeks after initial treatment, depending on the study, to analyze monkey tau mRNA and protein in different CNS tissues. Tissue homogenates were generated from full regions of the spinal cord—cervical, thoracic, and lumbar—and full brain regions—frontal cortex, temporal cortex, and hippocampus. Monkey tau protein was also measured in CSF that was drawn just before initial dosing as well as at necropsy.

Statistics

The data were analyzed for statistical significance using the graphing program GraphPad Prism 6. To determine sample size for tau reduction and pathology, a pilot cohort of $n = 5$ per treatment was analyzed and found to be sufficient to see significant differences in tau expression and pathology. Each study was completed with the listed number of mice in the figure legends. Two-tailed Student's t tests were used for sarkosyl and SDD-AGE blot quantifications. One-way ANOVA with Sidak post hoc analyses were used for saline versus scrambled mRNA analysis, total tau protein expression, AT8 pathology quantification, Thioflavin S pathology quantification, hippocampal volume and entorhinal area, DAPI counts and cell size analysis, tau seeding, nestlet weight, and monkey mRNA and protein analysis. For nestlet score, because the scoring was a nonordinal scale, a Kruskal-Wallis test was performed with Dunn's post hoc multiple comparison analysis. Two-way ANOVA with Bonferroni post hoc analyses were used for the duration of action study. A two-way repeated-measures ANOVA with Sidak post hoc analysis was used to analyze changes in CSF tau protein in cynomolgus monkeys with each monkey serving as its own baseline. Linear regression was used for the correlations between cynomolgus CSF and brain/spinal cord tau protein. Graphical data are represented as box and whisker plots with individual points overlaid, where error bars represent maximum and minimum values, and the boxed line represents the median.

SUPPLEMENTARY MATERIALS

www.sciencetranslationalmedicine.org/cgi/content/full/9/374/eaag0481/DC1

Fig. S1. Human and murine tau mRNA in control-treated PS19 mice.

Fig. S2. ASOs are distributed throughout adult mouse brain.

Fig. S3. Human tau mRNA is decreased after Tau^{ASO-12} treatment in the 6- to 9-month-old prevention cohort and 9- to 12-month-old reversal cohort.

Fig. S4. Phosphorylated tau is reversed across multiple brain regions after reducing human tau.

Fig. S5. Human tau reduction reverses Thioflavin S–positive NFTs in the piriform cortex of aged PS19 mice.

Fig. S6. Astrogliosis is reduced after Tau^{ASO-12} treatment in aged PS19 mice.
Fig. S7. Reducing human tau prevents entorhinal cortex atrophy in aged PS19 mice.
Fig. S8. Reducing human tau prevents a reduction in cell size in the CA1 region of the hippocampus in aged PS19 mice.
Fig. S9. Correlation of total tau protein between brain and CSF in nonhuman primates.

REFERENCES AND NOTES

1. H. Braak, E. Braak, Neuropathological stageing of Alzheimer-related changes. *Acta Neuropathol.* **82**, 239–259 (1991).
2. B. T. Hyman, G. W. Van Hoesen, A. R. Damasio, C. L. Barnes, Alzheimer's disease: Cell-specific pathology isolates the hippocampal formation. *Science* **225**, 1168–1170 (1984).
3. P. T. Nelson, I. Alafuzoff, E. H. Bigio, C. Bouras, H. Braak, N. J. Cairns, R. J. Castellani, B. J. Crain, P. Davies, K. Del Tredici, C. Duyckaerts, M. P. Frosch, V. Haroutunian, P. R. Hof, C. M. Hulette, B. T. Hyman, T. Iwatsubo, K. A. Jellinger, G. A. Jicha, E. Kövari, W. A. Kukull, J. B. Leverenz, S. Love, I. R. Mackenzie, D. M. Mann, E. Masliah, A. C. McKee, T. J. Montine, J. C. Morris, J. A. Schneider, J. A. Sonnen, D. R. Thal, J. Q. Trojanowski, J. C. Troncoso, T. Wisniewski, R. L. Woltjer, T. G. Beach, Correlation of Alzheimer disease neuropathologic changes with cognitive status: A review of the literature. *J. Neuropathol. Exp. Neurol.* **71**, 362–381 (2012).
4. M. Hosokawa, T. Arai, M. Masuda-Suzukake, T. Nonaka, M. Yamashita, H. Akiyama, M. Hasegawa, Methylene blue reduced abnormal tau accumulation in P301L tau transgenic mice. *PLOS ONE* **7**, e52389 (2012).
5. S.-W. Min, X. Chen, T. E. Tracy, Y. Li, Y. Zhou, C. Wang, K. Shirakawa, S. S. Minami, E. Defensor, S. A. Mok, P. D. Sohn, B. Schilling, X. Cong, L. Ellerby, B. W. Gibson, J. Johnson, N. Krogan, M. Shamloo, J. Gestwicki, E. Masliah, E. Verdin, L. Gan, Critical role of acetylation in tau-mediated neurodegeneration and cognitive deficits. *Nat. Med.* **21**, 1154–1162 (2015).
6. N. Myeku, C. L. Clelland, S. Emrani, N. V. Kukushkin, W. H. Yu, A. L. Goldberg, K. E. Duff, Tau-driven 26S proteasome impairment and cognitive dysfunction can be prevented early in disease by activating cAMP-PKA signaling. *Nat. Med.* **22**, 46–53 (2016).
7. K. Yanamandra, N. Kfoury, H. Jiang, T. E. Mahan, S. Ma, S. E. Maloney, D. F. Wozniak, M. I. Diamond, D. M. Holtzman, Anti-tau antibodies that block tau aggregate seeding in vitro markedly decrease pathology and improve cognition in vivo. *Neuron* **80**, 402–414 (2013).
8. D. L. Castillo-Carranza, U. Sengupta, M. J. Guerrero-Muñoz, C. A. Lasagna-Reeves, J. E. Gerson, G. Singh, D. M. Estes, A. D. T. Barrett, K. T. Dineley, G. R. Jackson, R. Kayed, Passive immunization with tau oligomer monoclonal antibody reverses tauopathy phenotypes without affecting hyperphosphorylated neurofibrillary tangles. *J. Neurosci.* **34**, 4260–4272 (2014).
9. M. Bi, A. Ittner, Y. D. Ke, J. Götz, L. M. Ittner, Tau-targeted immunization impedes progression of neurofibrillary histopathology in aged P301L tau transgenic mice. *PLOS ONE* **6**, e26860 (2011).
10. M. Boimel, N. Grigoriadis, A. Lourbopoulos, E. Haber, O. Abramsky, H. Rosenmann, Efficacy and safety of immunization with phosphorylated tau against neurofibrillary tangles in mice. *Exp. Neurol.* **224**, 472–485 (2010).
11. A. Ittner, J. Bertz, L. S. Suh, C. H. Stevens, J. Götz, L. M. Ittner, Tau-targeting passive immunization modulates aspects of pathology in tau transgenic mice. *J. Neurochem.* **132**, 135–145 (2015).
12. P. Lei, S. Ayton, D. I. Finkelstein, L. Spoerri, G. D. Ciccotosto, D. K. Wright, B. X. W. Wong, P. A. Adlard, R. A. Cherny, L. Q. Lam, B. R. Roberts, I. Volitakis, G. F. Egan, C. A. McLean, R. Cappai, J. A. Duce, A. I. Bush, Tau deficiency induces parkinsonism with dementia by impairing APP-mediated iron export. *Nat. Med.* **18**, 291–295 (2012).
13. M. Morris, P. Hamto, A. Adame, N. Devidze, E. Masliah, L. Mucke, Age-appropriate cognition and subtle dopamine-independent motor deficits in aged *tau* knockout mice. *Neurobiol. Aging* **34**, 1523–1529 (2013).
14. Z. Li, A. M. Hall, M. Kelinske, E. D. Roberson, Seizure resistance without parkinsonism in aged mice after tau reduction. *Neurobiol. Aging* **35**, 2617–2624 (2014).
15. S. L. DeVos, D. K. Goncharoff, G. Chen, C. S. Kebodeaux, K. Yamada, F. R. Stewart, D. R. Schuler, S. E. Maloney, D. F. Wozniak, F. Rigo, C. F. Bennett, J. R. Cirrito, D. M. Holtzman, T. M. Miller, Antisense reduction of tau in adult mice protects against seizures. *J. Neurosci.* **33**, 12887–12897 (2013).
16. R. A. Smith, T. M. Miller, K. Yamanaka, B. P. Monia, T. P. Condon, G. Hung, C. S. Lobsiger, C. M. Ward, M. McAlonis-Downes, H. Wei, E. V. Wancewicz, C. F. Bennett, D. W. Cleveland, Antisense oligonucleotide therapy for neurodegenerative disease. *J. Clin. Invest.* **116**, 2290–2296 (2006).
17. H. B. Kordasiewicz, L. M. Stanek, E. V. Wancewicz, C. Mazur, M. M. McAlonis, K. A. Pytel, J. W. Artates, A. Weiss, S. H. Cheng, L. S. Shihabuddin, G. Hung, C. F. Bennett, D. W. Cleveland, Sustained therapeutic reversal of Huntington's disease by transient repression of huntingtin synthesis. *Neuron* **74**, 1031–1044 (2012).
18. K. M. Schoch, S. L. DeVos, R. L. Miller, S. J. Chun, M. Norrbom, D. F. Wozniak, H. N. Dawson, C. F. Bennett, F. Rigo, T. M. Miller, Increased 4R-tau induces pathological changes in a human-tau mouse model. *Neuron* **90**, 941–947 (2016).
19. C. Lagier-Tourenne, M. Baughn, F. Rigo, S. Sun, P. Liu, H.-R. Li, J. Jiang, A. T. Watt, S. Chun, M. Katz, J. Qiu, Y. Sun, S.-C. Ling, Q. Zhu, M. Polymenidou, K. Drenner, J. W. Artates, M. McAlonis-Downes, S. Markmiller, K. R. Hutt, D. P. Pizzo, J. Cady, M. B. Harms, R. H. Baloh, S. R. Vandenberg, G. W. Yeo, X.-D. Fu, C. F. Bennett, D. W. Cleveland, J. Ravits, Targeted degradation of sense and antisense *C9orf72* RNA foci as therapy for ALS and frontotemporal degeneration. *Proc. Natl. Acad. Sci. U.S.A.* **110**, E4530–E4539 (2013).
20. C. J. Donnelly, P.-W. Zhang, J. T. Pham, A. R. Haeusler, A. R. Heusler, N. A. Mistry, S. Vidensky, E. L. Daley, E. M. Poth, B. Hoover, D. M. Fines, N. Maragakis, P. J. Tienari, L. Petrucelli, B. J. Traynor, J. Wang, F. Rigo, C. F. Bennett, S. Blackshaw, R. Sattler, J. D. Rothstein, RNA toxicity from the ALS/FTD *C9ORF72* expansion is mitigated by antisense intervention. *Neuron* **80**, 415–428 (2013).
21. T. M. Miller, A. Pestronk, W. David, J. Rothstein, E. Simpson, S. H. Appel, P. L. Andres, K. Mahoney, P. Allred, K. Alexander, L. W. Ostrow, D. Schoenfeld, E. A. Macklin, D. A. Norris, G. Manousakis, M. Crisp, R. Smith, C. F. Bennett, K. M. Bishop, M. E. Cudkowicz, An antisense oligonucleotide against *SOD1* delivered intrathecally for patients with *SOD1* familial amyotrophic lateral sclerosis: A phase 1, randomised, first-in-man study. *Lancet Neurol.* **12**, 435–442 (2013).
22. Y. Yoshiyama, M. Higuchi, B. Zhang, S.-M. Huang, N. Iwata, T. C. Saido, J. Maeda, T. Suhara, J. Q. Trojanowski, V. M.-Y. Lee, Synapse loss and microglial activation precede tangles in a P301S tauopathy mouse model. *Neuron* **53**, 337–351 (2007).
23. Y.-J. Lee, S. B. Han, S.-Y. Nam, K.-W. Oh, J. T. Hong, Inflammation and Alzheimer's disease. *Arch. Pharm. Res.* **33**, 1539–1556 (2010).
24. T. C. Frank-Cannon, L. T. Alto, F. E. McAlpine, M. G. Tansey, Does neuroinflammation fan the flame in neurodegenerative diseases? *Mol. Neurodegener.* **4**, 47 (2009).
25. A. Saul, F. Sprenger, T. A. Bayer, O. Wirths, Accelerated tau pathology with synaptic and neuronal loss in a novel triple transgenic mouse model of Alzheimer's disease. *Neurobiol. Aging* **34**, 2564–2573 (2013).
26. B. B. Holmes, S. L. DeVos, N. Kfoury, M. Li, R. Jacks, K. Yanamandra, M. O. Ouidja, F. M. Brodsky, J. Marasa, D. P. Bagchi, P. T. Kotzbauer, T. M. Miller, D. Papy-Garcia, M. I. Diamond, Heparan sulfate proteoglycans mediate internalization and propagation of specific proteopathic seeds. *Proc. Natl. Acad. Sci. U.S.A.* **110**, E3138–E3147 (2013).
27. A. de Calignon, M. Polydoro, M. Suárez-Calvet, C. William, D. H. Adamowicz, K. J. Kopeikina, R. Pitstick, N. Sahara, K. H. Ashe, G. A. Carlson, T. L. Spires-Jones, B. T. Hyman, Propagation of tau pathology in a model of early Alzheimer's disease. *Neuron* **73**, 685–697 (2012).
28. L. Liu, V. Drouet, J. W. Wu, M. P. Witter, S. A. Small, C. Clelland, K. Duff, Trans-synaptic spread of tau pathology in vivo. *PLOS ONE* **7**, e31302 (2012).
29. L. C. Walker, M. I. Diamond, K. E. Duff, B. T. Hyman, Mechanisms of protein seeding in neurodegenerative diseases. *JAMA Neurol.* **70**, 304–310 (2013).
30. B. B. Holmes, J. L. Furman, T. E. Mahan, T. R. Yamasaki, H. Mirbaha, W. C. Eades, L. Belaygorod, N. J. Cairns, D. M. Holtzman, M. I. Diamond, Proteopathic tau seeding predicts tauopathy in vivo. *Proc. Natl. Acad. Sci. U.S.A.* **111**, E4376–E4385 (2014).
31. J. L. Furman, B. B. Holmes, M. I. Diamond, Sensitive detection of proteopathic seeding activity with FRET flow cytometry. *J. Vis. Exp.* e53205 (2015).
32. V. Torres-Lista, L. Giménez-Llort, Impairment of nesting behaviour in 3xTg-AD mice. *Behav. Brain Res.* **247**, 153–157 (2013).
33. K. Yamada, J. K. Holth, F. Liao, F. R. Stewart, T. E. Mahan, H. Jiang, J. R. Cirrito, T. K. Patel, K. Hochgräfe, E.-M. Mandelkow, D. M. Holtzman, Neuronal activity regulates extracellular tau in vivo. *J. Exp. Med.* **211**, 387–393 (2014).
34. A. Lleó, E. Cavedo, L. Parnetti, H. Vanderstichele, S. K. Herukka, N. Andreasen, R. Ghidoni, P. Lewczuk, A. Jeromin, B. Winblad, M. Tsolaki, B. Mroczko, P. J. Visser, I. Santana, P. Svenningsson, K. Blennow, D. Aarsland, J. L. Molinuevo, H. Zetterberg, B. Mollenhauer, Cerebrospinal fluid biomarkers in trials for Alzheimer and Parkinson diseases. *Nat. Rev. Neurol.* **11**, 41–55 (2015).
35. M. Polydoro, A. de Calignon, M. Suárez-Calvet, L. Sanchez, K. R. Kay, S. B. Nicholls, A. D. Roe, R. Pitstick, G. A. Carlson, T. Gómez-Isla, T. L. Spires-Jones, B. T. Hyman, Reversal of neurofibrillary tangles and tau-associated phenotype in the rTgTauEC model of early Alzheimer's disease. *J. Neurosci.* **33**, 13300–13311 (2013).
36. K. Santacruz, J. Lewis, T. Spires, J. Paulson, L. Kotilinek, M. Ingelsson, A. Guimaraes, M. DeTure, M. Ramsden, E. McGowan, C. Forster, M. Yue, J. Orne, C. Janus, A. Mariash, M. Kuskowski, B. Hyman, M. Hutton, K. H. Ashe, Tau suppression in a neurodegenerative mouse model improves memory function. *Science* **309**, 476–481 (2005).
37. M. Dumont, C. Stack, C. Elipenahli, S. Jainuddin, M. Gerges, N. N. Starkova, L. Yang, A. A. Starkov, F. Beal, Behavioral deficit, oxidative stress, and mitochondrial dysfunction precede tau pathology in P301S transgenic mice. *FASEB J.* **25**, 4063–4072 (2011).
38. H. Takeuchi, M. Iba, H. Inoue, M. Higuchi, K. Takao, K. Tsukita, Y. Karatsu, Y. Iwamoto, T. Miyakawa, T. Suhara, J. Q. Trojanowski, V. M.-Y. Lee, R. Takahashi, P301S mutant human tau transgenic mice manifest early symptoms of human tauopathies with dementia and altered sensorimotor gating. *PLOS ONE* **6**, e21050 (2011).

39. G. R. Mallucci, M. D. White, M. Farmer, A. Dickinson, H. Khatun, A. D. Powell, S. Brandner, J. G. R. Jefferys, J. Collinge, Targeting cellular prion protein reverses early cognitive deficits and neurophysiological dysfunction in prion-infected mice. *Neuron* **53**, 325–335 (2007).
40. G. U. Höglinger, N. M. Melhem, D. W. Dickson, P. M. A. Sleiman, L.-S. Wang, L. Klei, R. Rademakers, R. de Silva, I. Litvan, D. E. Riley, J. C. van Swieten, P. Heutink, Z. K. Wszolek, R. J. Uitti, J. Vandrovcova, H. I. Hurtig, R. G. Gross, W. Maetzler, S. Goldwurm, E. Tolosa, B. Borroni, P. Pastor; PSP Genetics Study Group, L. B. Cantwell, M. R. Han, A. Dillman, M. P. van der Brug, J. R. Gibbs, M. R. Cookson, D. G. Hernandez, A. B. Singleton, M. J. Farrer, C.-E. Yu, L. I. Golbe, T. Revesz, J. Hardy, A. J. Lees, B. Devlin, H. Hakonarson, U. Müller, G. D. Schellenberg, Identification of common variants influencing risk of the tauopathy progressive supranuclear palsy. *Nat. Genet.* **43**, 699–705 (2011).
41. A. L. Boxer, A. E. Lang, M. Grossman, D. S. Knopman, B. L. Miller, L. S. Schneider, R. S. Doody, A. Lees, L. I. Golbe, D. R. Williams, J.-C. Corvol, A. Ludolph, D. Burn, S. Lorenzl, I. Litvan, E. D. Roberson, G. U. Höglinger, M. Koestler, C. R. Jack Jr., V. Van Deerlin, C. Randolph, I. V Lobach, H. W. Heuer, I. Gozes, L. Parker, S. Whitaker, J. Hirman, A. J. Stewart, M. Gold, B. H. Morimoto; AL-108-231 Investigators, Davunetide in patients with progressive supranuclear palsy: A randomised, double-blind, placebo-controlled phase 2/3 trial. *Lancet. Neurol.* **13**, 676–685 (2014).
42. J. C. Rojas, A. L. Boxer, Neurodegenerative disease in 2015: Targeting tauopathies for therapeutic translation. *Nat. Rev. Neurol.* **12**, 74–76 (2016).
43. M. Goedert, B. Ghetti, M. G. Spillantini, Frontotemporal dementia: Implications for understanding Alzheimer disease. *Cold Spring Harb. Perspect. Med.* **2**, a006254 (2012).
44. D. T. Chien, S. Bahri, A. K. Szardenings, J. C. Walsh, F. Mu, M.-Y. Su, W. R. Shankle, A. Elizarov, H. C. Kolb, Early clinical PET imaging results with the novel PHF-tau radioligand [F-18]-T807. *J. Alzheimers Dis.* **34**, 457–468 (2013).
45. I. Santa-Maria, A. Haggiagi, X. Liu, J. Wasserscheid, P. T. Nelson, K. Dewar, L. N. Clark, J. F. Crary, The *MAPT* H1 haplotype is associated with tangle-predominant dementia. *Acta Neuropathol.* **124**, 693–704 (2012).
46. C. Cruchaga, J. S. K. Kauwe, O. Harari, S. C. Jin, Y. Cai, C. M. Karch, B. A. Benitez, A. T. Jeng, T. Skorupa, D. Carrell, S. Bertelsen, M. Bailey, D. McKean, J. M. Shulman, P. L. De Jager, L. Chibnik, D. A. Bennett, S. E. Arnold, D. Harold, R. Sims, A. Gerrish, J. Williams, V. M. Van Deerlin, V. M.-Y. Lee, L. M. Shaw, J. Q. Trojanowski, J. L. Haines, R. Mayeux, M. A. Pericak-Vance, L. A. Farrer, G. D. Schellenberg, E. R. Peskind, D. Galasko, A. M. Fagan, D. M. Holtzman, J. C. Morris; GERAD Consortium, Alzheimer's Disease Neuroimaging Initiative (ADNI), Alzheimer Disease Genetic Consortium (ADGC), A. M. Goate, GWAS of cerebrospinal fluid tau levels identifies risk variants for Alzheimer's disease. *Neuron* **78**, 256–268 (2013).
47. R. S. Desikan, A. J. Schork, Y. Wang, A. Witoelar, M. Sharma, L. K. McEvoy, D. Holland, J. B. Brewer, C.-H. Chen, W. K. Thompson, D. Harold, J. Williams, M. J. Owen, M. C. O'Donovan, M. A. Pericak-Vance, R. Mayeux, J. L. Haines, L. A. Farrer, G. D. Schellenberg, P. Heutink, A. B. Singleton, A. Brice, N. W. Wood, J. Hardy, M. Martinez, S. H. Choi, A. DeStefano, M. A. Ikram, J. C. Bis, A. Smith, A. L. Fitzpatrick, L. Launer, C. van Duijn, S. Seshadri, I. D. Ulstein, D. Aarsland, T. Fladby, S. Djurovic, B. T. Hyman, J. Snaedal, H. Stefansson, K. Stefansson, T. Gasser, O. A. Andreassen, A. M. Dale; ADNI, ADGC, GERAD, CHARGE and IPDGC Investigators, Genetic overlap between Alzheimer's disease and Parkinson's disease at the MAPT locus. *Mol. Psychiatry* **20**, 1588–1595 (2015).
48. Y. Zhao, I.-C. Tseng, C. J. Heyser, E. Rockenstein, M. Mante, A. Adame, Q. Zheng, T. Huang, X. Wang, P. E. Arslan, P. Chakrabarty, C. Wu, G. Bu, W. C. Mobley, Y.-w. Zhang, P. St George-Hyslop, E. Masliah, P. Fraser, H. Xu, Appoptosin-mediated caspase cleavage of tau contributes to progressive supranuclear palsy pathogenesis. *Neuron* **87**, 963–975 (2015).
49. A. Kondo, K. Shahpasand, R. Mannix, J. Qiu, J. Moncaster, C.-H. Chen, Y. Yao, Y.-M. Lin, J. A. Driver, Y. Sun, S. Wei, M.-L. Luo, O. Albayram, P. Huang, A. Rotenberg, A. Ryo, L. E. Goldstein, A. Pascual-Leone, A. C. McKee, W. Meehan, X. Z. Zhou, K. P. Lu, Antibody against early driver of neurodegeneration *cis* P-tau blocks brain injury and tauopathy. *Nature* **523**, 431–436 (2015).
50. E. D. Roberson, K. Scearce-Levie, J. J. Palop, F. Yan, I. H. Cheng, T. Wu, H. Gerstein, G.-Q. Yu, L. Mucke, Reducing endogenous tau ameliorates amyloid β-induced deficits in an Alzheimer's disease mouse model. *Science* **316**, 750–754 (2007).
51. E. D. Roberson, B. Halabisky, J. W. Yoo, J. Yao, J. Chin, F. Yan, T. Wu, P. Hamto, N. Devidze, G.-Q. Yu, J. J. Palop, J. L. Noebels, L. Mucke, Amyloid-β/Fyn–induced synaptic, network, and cognitive impairments depend on tau levels in multiple mouse models of Alzheimer's disease. *J. Neurosci.* **31**, 700–711 (2011).
52. K. A. Vossel, K. Zhang, J. Brodbeck, A. C. Daub, P. Sharma, S. Finkbeiner, B. Cui, L. Mucke, Tau reduction prevents Aβ-induced defects in axonal transport. *Science* **330**, 198 (2010).
53. K. Leroy, K. Ando, V. Laporte, R. Dedecker, V. Suain, M. Authelet, C. Héraud, N. Pierrot, Z. Yilmaz, J.-N. Octave, J.-P. Brion, Lack of tau proteins rescues neuronal cell death and decreases amyloidogenic processing of APP in *APP/PS1* mice. *Am. J. Pathol.* **181**, 1928–1940 (2012).
54. L. M. Ittner, Y. D. Ke, F. Delerue, M. Bi, A. Gladbach, J. van Eersel, H. Wölfing, B. C. Chieng, M. J. Christie, I. A. Napier, A. Eckert, M. Staufenbiel, E. Hardeman, J. Götz, Dendritic function of tau mediates amyloid-β toxicity in Alzheimer's disease mouse models. *Cell* **142**, 387–397 (2010).
55. E. Suberbielle, P. E. Sanchez, A. V. Kravitz, X. Wang, K. Ho, K. Eilertson, N. Devidze, A. C. Kreitzer, L. Mucke, Physiologic brain activity causes DNA double-strand breaks in neurons, with exacerbation by amyloid-β. *Nat. Neurosci.* **16**, 613–621 (2013).
56. A. van Hummel, M. Bi, S. Ippati, J. van der Hoven, A. Volkerling, W. S. Lee, D. C. S. Tan, A. Bongers, A. Ittner, Y. D. Ke, L. M. Ittner, No overt deficits in aged tau-deficient C57Bl/6.*Mapt*$^{tm1(EGFP)Klt}$ GFP knockin mice. *PLOS ONE* **11**, e0163236 (2016).
57. M. A. Passini, J. Bu, A. M. Richards, C. Kinnecom, S. P. Sardi, L. M. Stanek, Y. Hua, F. Rigo, J. Matson, G. Hung, E. M. Kaye, L. S. Shihabuddin, A. R. Krainer, C. F. Bennett, S. H. Cheng, Antisense oligonucleotides delivered to the mouse CNS ameliorate symptoms of severe spinal muscular atrophy. *Sci. Transl. Med.* **3**, 72ra18 (2011).
58. C. A. Chiriboga, K. J. Swoboda, B. T. Darras, S. T. Iannaccone, J. Montes, D. C. De Vivo, D. A. Norris, C. F. Bennett, K. M. Bishop, Results from a phase 1 study of nusinersen (ISIS-SMN$_{Rx}$) in children with spinal muscular atrophy. *Neurology* **86**, 890–897 (2016).
59. S. L. DeVos, T. M. Miller, Antisense oligonucleotides: Treating neurodegeneration at the level of RNA. *Neurotherapeutics* **10**, 486–497 (2013).
60. R. A. McKay, L. J. Miraglia, L. L. Cummins, S. R. Owens, H. Sasmor, N. M. Dean, Characterization of a potent and specific class of antisense oligonucleotide inhibitor of human protein kinase C-α expression. *J. Biol. Chem.* **274**, 1715–1722 (1999).
61. S. L. DeVos, T. M. Miller, Direct intraventricular delivery of drugs to the rodent central nervous system. *J. Visualized Exp.* e50326 (2013).
62. S. Wegmann, E. A. Maury, M. J. Kirk, L. Saqran, A. Roe, S. L. DeVos, S. Nicholls, Z. Fan, S. Takeda, O. Cagsal-Getkin, C. M. William, T. L. Spires-Jones, R. Pitstick, G. A. Carlson, A. M. Pooler, B. T. Hyman, Removing endogenous tau does not prevent tau propagation yet reduces its neurotoxicity. *EMBO J.* **34**, 3028–3041 (2015).
63. D. W. Sanders, S. K. Kaufman, S. L. DeVos, A. M. Sharma, H. Mirbaha, A. Li, S. J. Barker, A. C. Foley, J. R. Thorpe, L. C. Serpell, T. M. Miller, L. T. Grinberg, W. W. Seeley, M. I. Diamond, Distinct tau prion strains propagate in cells and mice and define different tauopathies. *Neuron* **82**, 1271–1288 (2014).
64. S. Takeda, S. Wegmann, H. Cho, S. L. DeVos, C. Commins, A. D. Roe, S. B. Nicholls, G. A. Carlson, R. Pitstick, C. K. Nobuhara, I. Costantino, M. P. Frosch, D. J. Müller, D. Irimia, B. T. Hyman, Neuronal uptake and propagation of a rare phosphorylated high-molecular-weight tau derived from Alzheimer's disease brain. *Nat. Commun.* **6**, 8490 (2015).
65. S. Takeda, C. Commins, S. L. DeVos, C. K. Nobuhara, S. Wegmann, A. D. Roe, I. Costantino, Z. Fan, S. B. Nicholls, A. E. Sherman, A. T. Trisini Lipsanopoulos, C. R. Scherzer, G. A. Carlson, R. Pitstick, E. R. Peskind, M. A. Raskind, G. Li, T. J. Montine, M. P. Frosch, B. T. Hyman, Seed-competent high-molecular-weight tau species accumulates in the cerebrospinal fluid of Alzheimer's disease mouse model and human patients. *Ann. Neurol.* **80**, 355–367 (2016).
66. R. Deacon, Assessing burrowing, nest construction, and hoarding in mice. *J. Visualized Exp.* **2012**, e2607 (2012).

Acknowledgments: We thank T. Mahan and D. Holtzman for their help with analyzing hippocampal volume and quantifying AT8 pathology, E. Fisher for her help with manuscript revisions, S. Wegmann for her help with the Thioflavin S and sarkosyl protocol and edits on figures, B. T. Hyman for providing technical support with imaging Thioflavin S tissue in his laboratory and running SDD-AGE and sarkosyl experiments, and A. Plotzker for assistance with immunohistochemistry in PS19 mice. Ionis Pharmaceuticals supplied the authors with all of the ASOs in the described work. **Funding:** This work was supported by the Tau Consortium (to M.I.D. and T.M.M.), the NIH [P50 AG05681 to T.M.M. (principal investigator, J.C. Morris), National Institute of Neurological Disorders and Stroke (NINDS) (R01NS078398 to T.M.M.), and National Institute on Aging (R21AG044719-01 to T.M.M.)], CurePSP (to T.M.M.), and a Paul B. Beeson Career Development Award (NINDS K08NS074194 to T.M.M.). The microscopy work was supported by the Hope Center Alafi Neuroimaging Laboratory and P30 Neuroscience Blueprint Interdisciplinary Center Core award to Washington University (P30 NS057105).
Author contributions: S.L.D., H.B.K., C.F.B., and T.M.M. conceived and designed the murine experiments and wrote the manuscript. H.B.K., E.E.S., and C.F.B. conceived and designed the nonhuman primate experiments. The following authors carried out experiments and collected data: S.L.D. [Figs. 1 (A to J), 2 (A to Q), 3 (A to D), and 4 (A to H), and figs. S1 (A and B), S2, S3 (A and B), S4, S5, S6 (A to C), S7, and S8], R.L.M. [Figs. 1 (G to J), 2 (I to N), 3B, and 5 (A to C), and figs. S1 (A and B), S4, S6 (A to C), and S8], K.M.S. [Figs. 1 (G to J), 2 (L to N), 3A, and 5 (A to C), and figs. S1 (A and B), S5, S7, and S8], B.B.H. (Fig. 4, A to H), C.S.K. [Figs. 1 (C and G to J), 2 (I to N), and 3A], A.J.W. (Fig. 5, A to C), G.C. [Figs. 1 (A to C) and 2A, and fig. S1 (A and B)], T.S. (Fig. 5, A to C), H.T. (Fig. 6, A to I, and fig. S9, A to C), B.N. (Fig. 6, A to I, and fig. S9, A to C), and T.A.Z. (Fig. 6, A to I, and fig. S9, A to C). Once the experiments were completed and data were collected, S.L.D., R.L.M., B.B.H., H.B.K., M.I.D., and T.M.M. analyzed and interpreted the results. S.L.D. performed the statistical analyses, and M.I.D. and T.M.M. secured funding for all in vitro and in vivo murine projects. **Competing interests:** Both Ionis Pharmaceuticals and Washington University have

filed patents on the basis of using tau ASOs to treat CNS disorders. S.L.D., C.F.B., and T.M.M. are coinventors on patent #PCT/US2013/031500, "Methods for modulating tau expression for reducing neurodegenerative syndromes," and patent #61/719,149, "Methods for modulating tau expression." T.M.M. served on a medical advisory board for Ionis Pharmaceuticals and Biogen Idec and is a consultant for Cytokinetics. The other authors declare that they have no competing interests. **Data and materials availability:** No large scale data sets were generated in this study. The sequence of the ASOs used for both the murine work and nonhuman primate work is provided in Materials and Methods. The ASOs used in this study were made available by Ionis Pharmaceuticals through a material transfer agreement. ASOs can be made through a company such as Integrated DNA Technologies (*59*).

Submitted 19 October 2015
Resubmitted 13 May 2016
Accepted 17 November 2016
Published 25 January 2017
10.1126/scitranslmed.aag0481

Citation: S. L. DeVos, R. L. Miller, K. M. Schoch, B. B. Holmes, C. S. Kebodeaux, A. J. Wegener, G. Chen, T. Shen, H. Tran, B. Nichols, T. A. Zanardi, H. B. Kordasiewicz, E. E. Swayze, C. F. Bennett, M. I. Diamond, T. M. Miller, Tau reduction prevents neuronal loss and reverses pathological tau deposition and seeding in mice with tauopathy. *Sci. Transl. Med.* **9**, eaag0481 (2017).